2022

Direction Modulated Brachytherapy for the Treatment of Cervical Cancer

Dylan Richeson

Direction-Modulated Brachytherapy (DMBT) for the Treatment of Cervical Cancer

A thesis submitted in partial fulfillment of the requirements for the degree of Master of Science at Virginia Commonwealth University

By

Dylan Richeson

Bachelor of Science in Physics, Virginia Commonwealth University, May 2019

Advisor: William Y. Song, Ph.D.

Associate Professor

Department of Radiation Oncology

Virginia Commonwealth University

April, 2022

Acknowledgements

I would like to express my deepest gratitude to:

My committee members for their guidance

Dr. Gholami for her hard work

Dr. Song for his mentorship

My family for their love

Table of Contents

List of Figures

List of Tables

Abstract

Direction-Modulated Brachytherapy (DMBT) for the Treatment of Cervical Cancer

By

Dylan Richeson

Bachelor of Science in Physics, Virginia Commonwealth University, May 2019

Advisor: William Y. Song, Ph.D.

Associate Professor

Department of Radiation Oncology

Virginia Commonwealth University

April, 2022

P**urpose**: To evaluate and compare the performance of 9 experimental DMBT tandem models of varying physical dimensions in relation to 24 previously planned HDR cervical cancer treatment plans from multiple institutions that used conventional tandem and rings or ovoid applicators..

Methods and Materials: The DMBT tandem is designed to be used concurrently with IGABT and is made from an MRI-compatible tungsten-alloy rod with 6 channels grooved out of its periphery. 9 experimental DMBT tandem prototypes were provided. Each of the models were of equal lengths but varied in thickness, channel diameter size, and circle channel diameter size. Replanning was performed using our research TPS (BrachyVision® v.16.1, Varian, Palo Alto, CA). Inverse optimization using Acuros was performed for 12 patient cases (24 plans) belonging to three institutions: Virginia Commonwealth University, University of Michigan, and University of California San Diego. Original plans used conventional tandem and ovoids or ring applicators. Each of the 9 DMBT tandem models replaced the location of the original tandem such that the new dwell positions were at the level of the original plan's. The dwell positions of the ovoids or rings remained unchanged.

Results: The average relative reduction in D2cc using the thinnest DMBT tandem (model 1) were: -9.65% (ΔEQD2 $D2cc_{Bladder}$ = -3.6 Gy), -19.91% (ΔEQD2 $D2cc_{Rectum}$ = -3.87 Gy), and -14.55% (ΔEQD2 $D2cc_{Sigmoid}$ = -3.55 Gy), for the bladder, rectum, and sigmoid respectively. The average relative reduction in D2cc using the thickest DMBT tandem (model 9) were: -12.82% (ΔEQD2 $D2cc_{Bladder}$ = -4.05 Gy), -24.69% (ΔEQD2 $D2cc_{Rectum}$ = -4.05 Gy), and -18.42% (ΔEQD2 $D2cc_{Sigmoid}$ = -3.63 Gy), for the bladder, rectum, and sigmoid respectively.

Conclusions: Significant reductions in OAR dose while maintaining identical target coverage (D90) can be achieved by the use of any of the 9 DMBT tandem models. As DMBT tandem thickness increases, OAR dose decreases; however, there are no significant difference in

performance between models. Unless necessary to remain within an OAR's total dose (EQD2) limit, we advise the use of a moderately thick DMBT tandem (model 5) for clinical use as its physical dimensions resemble that of already used clinically conventional tandems while offering enhanced modulating capabilities.

KEYWORDS

Direction-modulated brachytherapy (DMBT), Image-guided adaptative brachytherapy (IGABT), organ-at-risk (OAR)

1. Introduction

1.1. Birth of Brachytherapy

The turn of the twentieth century was characterized by immense scientific discoveries that would affect the field of medicine and physics forever. One such discovery was that of radioactivity by Henri Becquerel in 1896. Shortly after, notable scientists such as Pierre Curie and Alexander Graham Bell suggested the use of this newly discovered property of radioactivity as a means of treating cancer and other malignant diseases. It was believed that this could be accomplished by implanting a radioisotope of radium into the body, near or around the site of the primary tumor. This proposed technique was first implemented in 1901 at the St. Louis Hospital in Paris where a patient suffering of lupus was treated using radium sulfate[1]. This treatment was amongst one of the earliest accounts of the technique commonly known as brachytherapy and marked the birth of the field of radiation therapy. In 1903, the first use of brachytherapy for the treatment of a gynecological disease was documented. In New York, a patient with cervical cancer was treated using 700 mg of radium bromide enclosed in glass tubing[1]. As the twentieth century progressed, technological advances complimented the growing field of radiation therapy. In the early century, X-ray machines were engineered to produce stronger and stronger energies. With the advent of nuclear reactors during World War II, the creation and use of artificially produced radionuclides such as cobalt 60 were incorporated for treatment purposes. By the 1970s the first medical linear accelerator was created and was able to produce even greater energies which have become a hallmark of modern day radiotherapy. However; despite these technological advancements in external beam radiation therapy (EBRT), brachytherapy still has its place and remains a standard of care for many cancers associated with the prostate, cervix, skin, lung, and

eyes. Brachytherapy, unlike external beam therapy, does not require ionizing radiation to traverse large depths of penetration in healthy tissue since the source is placed near or within the target. In addition, the average energy of common HDR sources are much lower than those used in external beam therapy resulting in steeper dose gradients. Low energy sources such as ^{192}Ir which emits photons with an average energy of approximately 380 keV are often used. The close proximity of the source to the target combined with its low average energy results in a high degrees of dose deposition in the target with minimal OAR and healthy tissue exposure.

1.2. Prognosis for Cervical Cancer

Cervical cancer is amongst the deadliest gynecological malignancies for women and is the leading cause of cancer mortality for women in developing countries [2]. This can be in part due to a lack of access to the human papillomavirus (HPV) vaccine as multiple strains of the virus can play a prominent role in the development of cancer. Mortality rates in the U.S from cervical cancer have decreased by 70% due to screening with the Pap test[3]. However, it still remains the 3rd most common gynecological malignancy in the U.S. Risk factors for developing cervical cancer include: early intercourse, multiple sexual partners, many pregnancies, smoking, immunosuppression, prenatal estrogen, and exposure to HPV 16 and/or 18[4]. Prescreening procedures such as the Pap test or Colposcopy may be used to identify the cancer early while vaccines such as Cervarix and Guardasil may be used to prevent it. The FIGO staging system determined by the International Federation of Gynecology Obstetrics allows physicians to define the extent of the disease and assign the appropriate treatment[5].

1.3. Historical Treatment of Cervical Cancer

As noted previously, brachytherapy has been used to treat cervical cancer since the beginning of the twentieth century; however, the technique of treatment planning has changed drastically. Due to the technological limitations of the 1930s, only 2D radiographic imaging could be used for treatment planning. From 2D images, prescription systems such as the Manchester system could be utilized. This system designated a point at which the prescription system should be delivered known as "point A". In 1938, the Manchester system defined the location of point A at 2 cm laterally from the center of the uterine canal and 2 cm superior of the mucosa membrane of the lateral fornix in the plane of the uterus. Often times the top edge of the ovoids were used as a surrogate for the fornix. The significance of this point lies in its proximity to the ureters which were believed to be the dose limiting structure in treatment planning. However, a major limitation of this prescription system is that point A is defined the same in all cases and doesn't take patient specific anatomy into account. It also relies on 2D imaging which doesn't account for the 3D spatial extent of the target and locations of nearby organs at risk (OAR), namely the bladder, rectum, and sigmoid colon. This lack of 3D information makes identifying the locations of OAR unrealistic and can lead to an increase likelihood of developing complications from treatment[7-9]. In conjunction with the point A prescription system, the famous Fletcher rules were utilized which defined various loading parameters (i.e. ratio of dwell times in various dwell positions based on the size of tandem and ovoids used) in order to produce the historic pear-shape dose distribution that has been associated with successful clinical outcomes[10-12]. However; one of the primary disadvantages of the Fletcher system is that it assumes that all tumors are of the same size and shape. Therefore, it does not account for cases of irregularly shaped tumors or ones that have extended to the pelvic side walls[11-12]. In modern times, external beam radiation

therapy (EBRT) followed by brachytherapy (BT) with or without concurrent chemotherapy has become the standard of care for the treatment of cervical cancer[10]. Despite the technological advancements of EBRT, it alone is not capable of delivering prescription doses without producing significant side effects such as inflammation, fibrosis, necrosis, and fistulas due to the proximity of nearby OARs[11]. This due to the increased depth of penetration required for ionizing radiation in EBRT to reach its target. In addition, the field size in much larger than in BT causing larger areas of healthy tissue to be irradiated. In BT, the source is placed inside the body within or near the target. In addition, the energy of the source is much lower than in EBRT. The combination of a lower energy and the closer proximity of the source to the target allows for high dose deposition within the tumor while providing a steep dose gradient that spares nearby OAR and surrounding healthy tissue.

1.4. Transition from 2D to 3D IGABT

With the advent of 3D imaging modalities such as CT and MRI, image-guided adaptive brachytherapy (IGABT) has become the favorable treatment planning technique over the point A prescription system. Multiple prospective and single institutional studies have shown that 3D IGABT can produce better local tumor control and reduce morbidity[13-15]. From the patient-specific volumetric information, the spatial position of the nearby OARs in relation to the high-risk clinical target volume (HRCTV) may be contoured in the treatment planning system. The Groupe Européen de Curiethérapie and Eurpoean Society for Radiotherapy and Oncology have created definitions for the HRCTV which would accommodate the transition from 2D to 3D IGABT. The HRCTV is defined to be at least the entirety of the cervix in addition to any other palpable extensions of the disease[16]. However, it becomes difficult to adhere to this definition

through the use of tandem and ovoid or ring applicators where it is difficult to confine the dose distribution in the anterior-posterior directions[17]. In order to circumvent this challenge, interstitial needles are often used which are capable of producing more conformal dose distribution by careful selection of their placement (dwell position) as well as the source's dwell times. The summation of the isotropic dose distribution created by interstitial needles in various dwell positions is summed with that produced by the tandem and ovoids/ring to create an anisotropic dose distribution. The use of needles are especially helpful in the case of locally advanced cervical cancer (LACC) for providing sufficient target coverage to laterally extended disease that is too far away from the dose emitted from common intracavitary applicators While interstitial needles are a useful tool for creating more conformal dose distributions, they are prone to many errors. Ideal needle placement can be difficult to accomplish due lack of experience and training on the part of the physician. To account for this, intracavitary-interstitial hybrid applicators may be used but they are still prone to positioning errors due to the flexing of the needles in the vaginal tissue. For these reasons, the exploration of alternative solutions have ensued.

1.5. Direction-Modulated Brachytherapy (DMBT)

Common intracavitary applicators still utilize an isotropic dose distribution; however, the high-risk clinical target volume (HRCTV) is often irregular in shape thus causing healthy tissue and OARs to receive unnecessary dose. In addition, if the disease extends superiorly into the uterus, then it will be difficult for the dose from the ovoids or rings to reach it. This means that the majority of the dose will come from the isotropic source in the tandem which has poor dose modulation. As discussed previously, one such solution to creating more conformal dose

distribution, is the use of interstitial needles; however, this technique is only applicable to larger HRCTV volumes in excess of 30 cm^3. For these reasons, there has been a growing interest into the implementation of a new anisotropic source that would complement the use of 3D imaging to create more conformal dose distributions[18-20]. This technique is known as direction-modulated brachy therapy (DMBT). Current work is being conducted in order to explore the possibility of utilizing an experimental tandem prototype that would be capable of producing an anisotropic dose distribution in line with the DMBT concept.

2. Purpose

The aim of our research is to evaluate and compare the performance of 9 experimental DMBT tandem models of varying physical dimensions in relation to 24 previously planned HDR cervical cancer treatment plans that used conventional tandem and rings or ovoids. We seek to identify the improvements in OAR doses, recto-vaginal (RV-RP) dose, the doses to the posterior-inferior border of symphysis (PIBS) reference points, and the equivalent total OAR doses delivered in 2 Gy fractions achieved by different DMBT tandem models for varying target sizes. We also seek to make recommendations for which model(s) should be used clinically.

3. Methodology

3.1. DMBT Tandem

The experimental DMBT tandem is designed with 6 channels bored out of the periphery of a non-ferromagnetic tungsten-alloy rod (ρ = 18.0 g/cm^3) and can be seen in Figure 1. The tungsten-alloy rod is composed of 95% tungsten, 3.5% nickel, and 1.5% copper[21]. The materials composing the alloy were carefully selected to be MRI compatible, creating minimal susceptibility artifact[22]. The density of tungsten is responsible for the modulation of the beam. Because the source channels are located at the periphery of the rod, radiation emitted towards the opposing side of the tandem will be attenuated with minimal transmission (16.5% for Ir-192 at 1 cm depth)[23]. In this study, 9 DMBT tandem models were evaluated and are shown in Figures 2-3. The models varied in regards to select physical dimensions (see Table 1 and Figure 4). Each model followed an identical 6 channel construction with equal tandem lengths of 80 mm while utilizing the same composition of tungsten-alloy material.

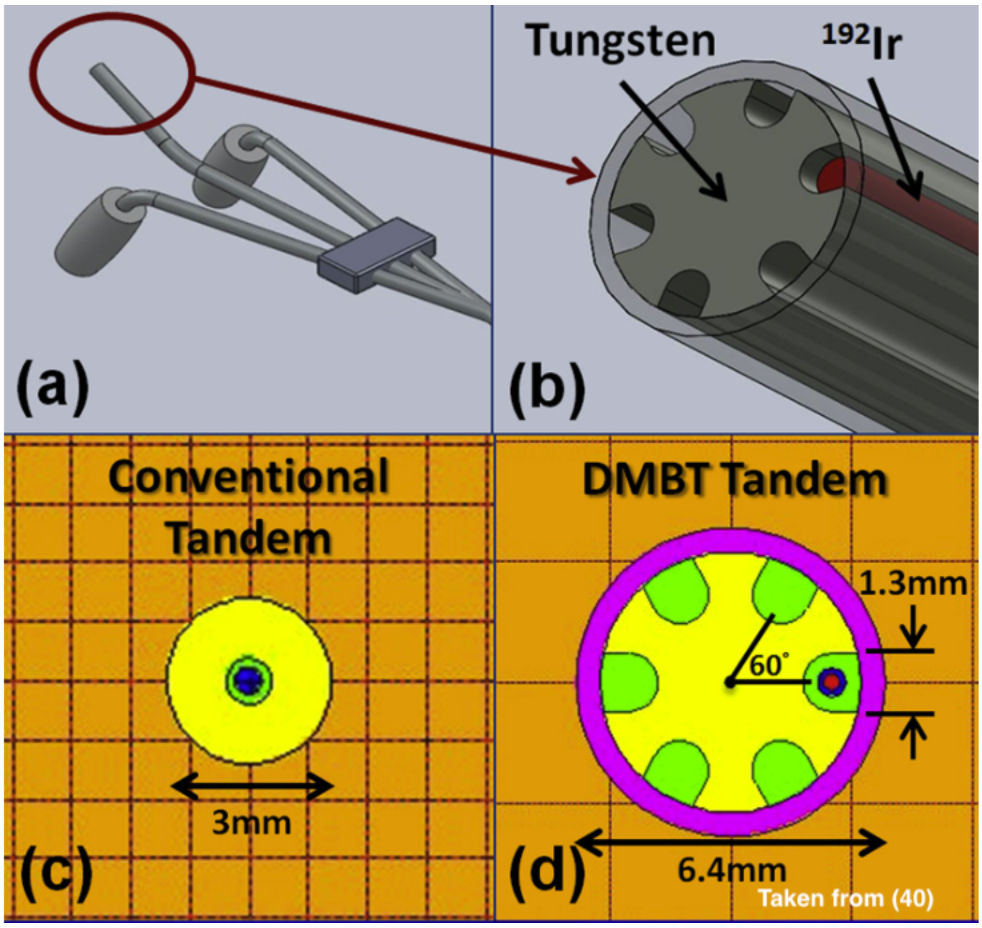

Figure 1. (a) A conventional tandem and ovoid applicator. (b) The direction-modulated brachytherapy (DMBT) tandem design with 6 peripheral holes born out of a non-ferromagnetic tungsten alloy. (c) A cross-section of a conventional tandem. (d) A cross-section of the DMBT tandem.

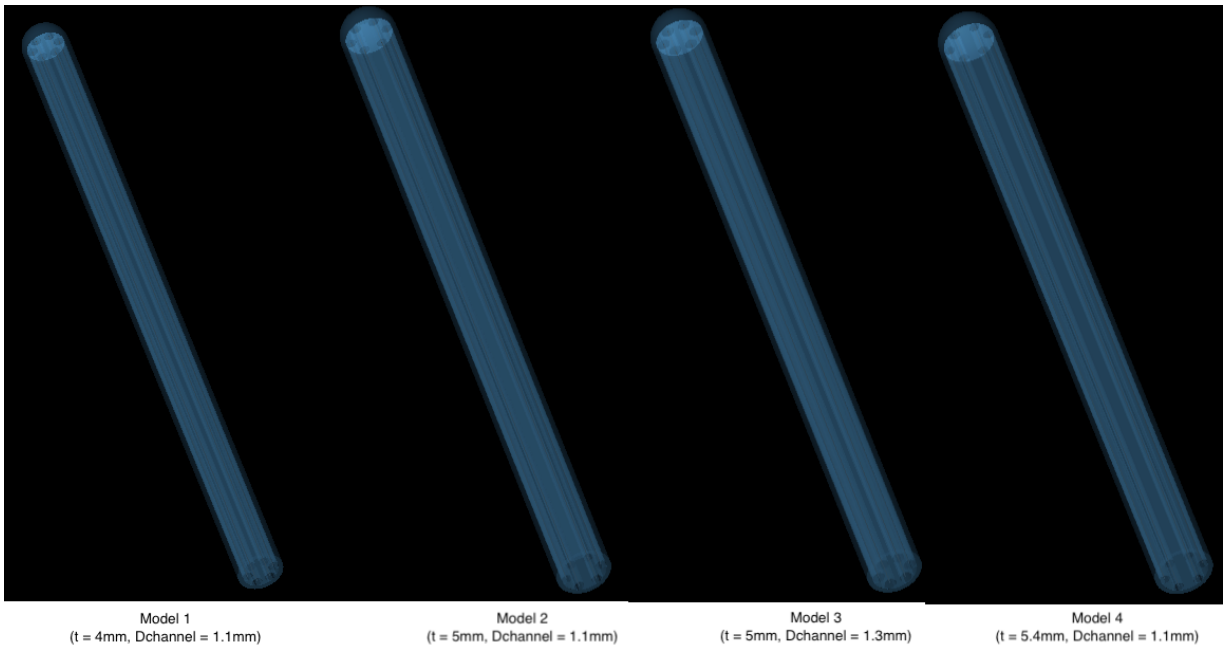

Figure 2. DMBT tandem models 1-4. Note the increase in thickness with increasing model number.

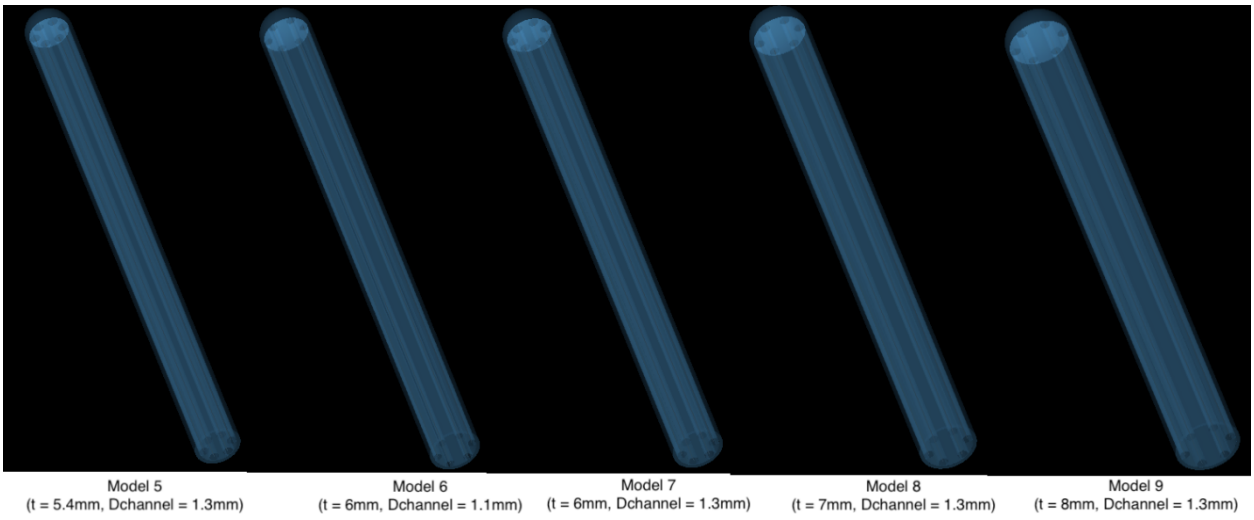

Figure 3. DMBT tandem models 5-9. Note the increase in thickness with increasing model number.

Model #	Thickness (t) [mm]	Channel diameter ($D_{channel}$) [mm]	Channel circle diameter [mm]
1	4	1.1	2.9
2	5	1.1	3.9
3	5	1.3	3.5
4	5.4	1.1	4.3
5	5.4	1.3	3.9
6	6	1.1	3.9
7	6	1.3	4.5
8	7	1.3	5.5
9	8	1.3	6.5

Table 1. The physical dimensions of all 9 DMBT tandem models in order of increasing tandem thickness and channel thickness. All models are 80 cm long.

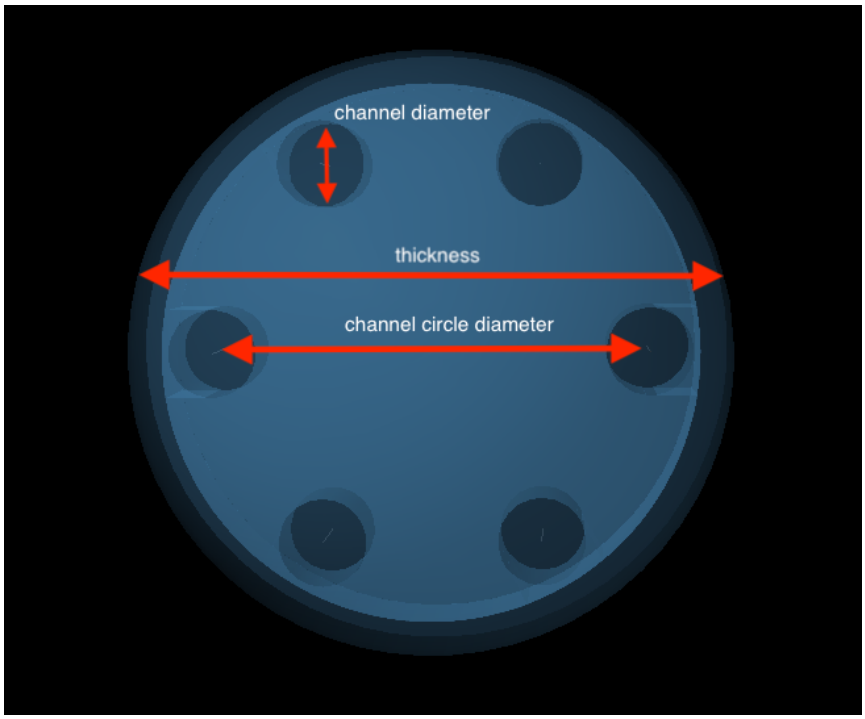

Figure 4 . Definitions of the physical dimensions of the DMBT tandem

3.2. Patient Cohort

A total 484 previously treated HDR cervical cancer treatment plans belonging to 96 patients was provided by three institutions: Virginia Commonwealth University (VCU), University of Michigan (UMich), and University of California San Diego (UCSD). The treatment plans selected for our study were filtered on four criteria. First, only plans containing all necessary import files were included. Second, plans that used intracavitary applicators only were selected. Third, since our patient population contained an insufficient number of patients simulated with MRI imaging, CT simulated only patients were selected. Lastly, only plans with straight or nearly straight tandems were selected. This consideration was made so that the straight prototype DMBT tandem could be aligned in the same position as the conventional tandem used by the original plan. Applying these considerations left us with a cohort of 24 previously treated CT based intracavitary plans (T&O and T&R) belonging to 12 patients. 4 patients with 14 total plans, 3 patients with 5 total plans, and 5 patients with 5 total plans belonged to UCSD, UMich, and VCU respectively. Of the original 24 plans, 8 plans used T&O and the remaining 17 used T&R. HRCTV sizes range from 7.71 cm^3 to 56.30 cm^3 with an average of 21.88 cm^3. Prescription doses ranged from 5.5 Gy to 7.5 Gy. FIGO stages ranged from IB1 to IVB. The number of fractions replanned with the DMBT tandem per patient ranged from 1 to 4. A summarized table of the patient cohort can be seen in Table 2.

Patient no.	FIGO stage	Average prescription dose [Gy]	Average HRCTV size [cm^3]	# of fractions replanned	Technique	Institution
1	IB1	7	9.54	3	T&O	UCSD
2	IIB	7	15.98	4	T&R	UCSD
3	IB3	7	65.72	4	T&R	UCSD
4	IIIC1	7.5	13.74	3	T&R	UCSD
5	IIB	7	15.35	1	T&R	UMich
6	IB2	5.67	27.21	3	T&R	UMich
7	IB2	6	18.64	1	T&O	VCU
8	IIB	6	56.3	1	T&O	VCU
9	IIA2	6	30.88	1	T&O	VCU
10	IVB	7	35.3	1	T&O	VCU
11	IIIB	6	42.79	1	T&O	VCU
12	IIB	6	44.82	1	T&O	VCU

Table 2 . Data on our 12 patient cohort used in our study. 17 plans belonged to 5 patients using T&R while the remaining 8 plans belonged to 7 patients using T&O. The # of fractions replanned represents only the number of fractions in which the DMBT tandem replaced the conventional tandem. For example, a patient may have had 4 fractions treated originally but we may have only have used the DMBT tandem in 2 of those fractions.

3.3. Sources and Afterloaders

In this study, two remote afterloaders were used including Varian's VariSource ix and GammaMed plus ix devices which used the VS200 Ir-192 (see Figure 5) and GammaMed Plus Ir-192 (GMP Ir-192) (see Figure 6) sources respectively. The treatment date for each plan was set to the calibration date of both sources which was 9/10/2020. The activity and source strength of the VS2000 Ir-192 model were 10 Ci and 40300 cGy•cm^2/h respectively. The activity and source strength of the GMP Ir-192 model were 10 Ci and 40700 cGy•cm^2/h respectively. Of the 12 patients, 9 (from VCU and UCSD) and 3 (from Umich) were treated with Varian's VariSource ix and GammaMed afterloaders ix respectively.

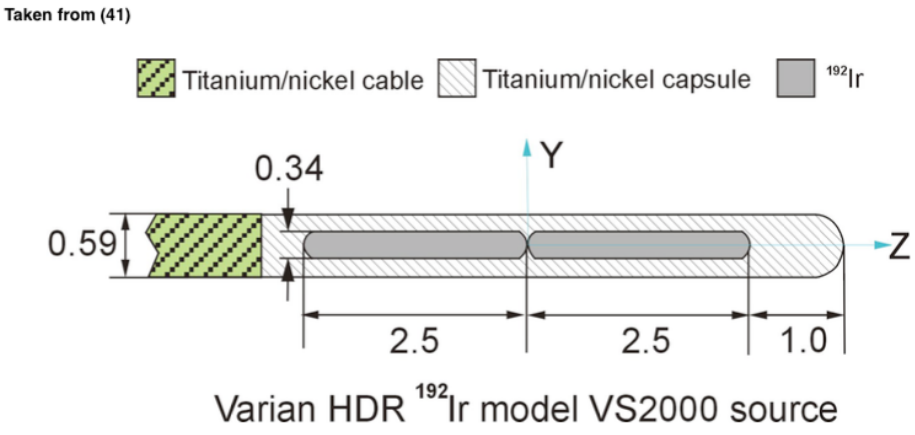

Figure 5. Materials and dimensions (mm) of the Varian Medical Systems VS2000 source[42]

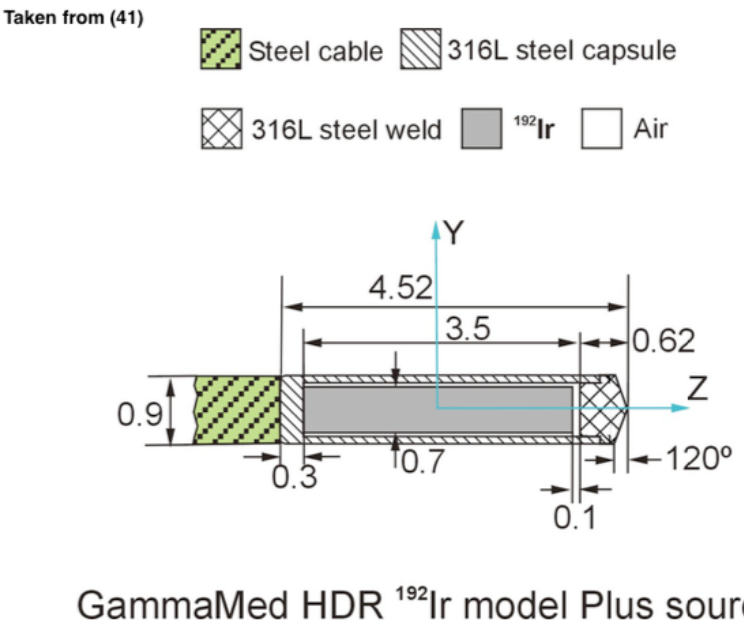

Figure 6. Materials and dimensions (mm) of the Varian Medical Systems VS2000 source[43]

3.4. Treatment Planning

3.4.1. Applicator Alignment

All 24 intracavitary treatment plans were imported into our research treatment planning system (BrachyVision® v.16.1, Varian, Palo Alto, CA) which contained all 9 DMBT tandem models (see Figure 7). Copies of the original plans were made for each of the 9 DMBT tandem models. The digitized DMBT tandem models were added to the original plans and aligned in the same position as the conventional tandem (see Figures 8-9). Once the DMBT tandem was successfully aligned, each dwell position in the six channels were at the same level as the dwell positions of the conventional tandem(see Figures 10-11). Dwell positions of the ovoids or rings remained unchanged.

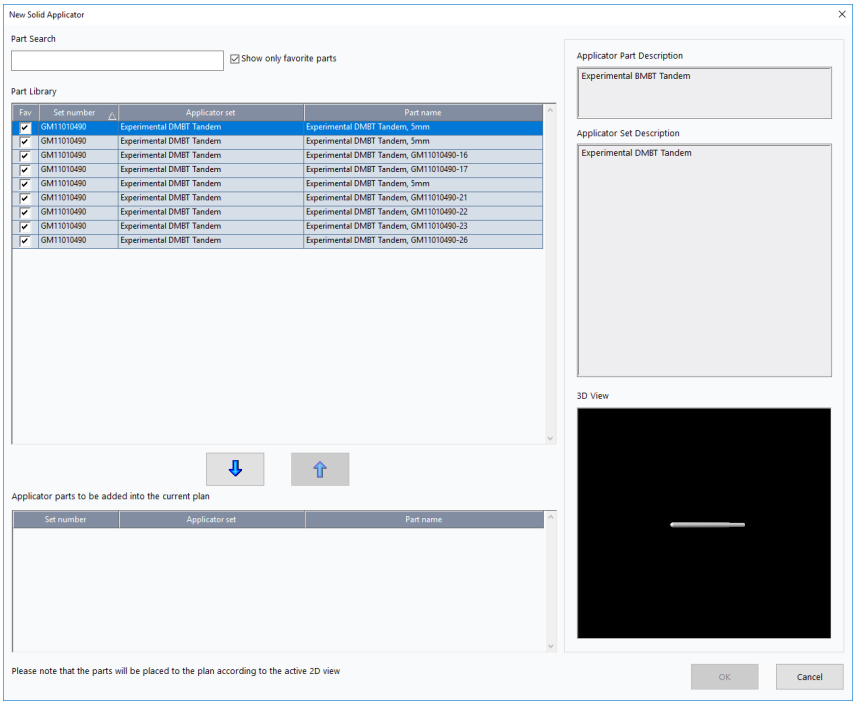

Figure 7 . Solid applicator menu containing all 9 DMBT tandem models in our research TPS's BrachyVision® software.

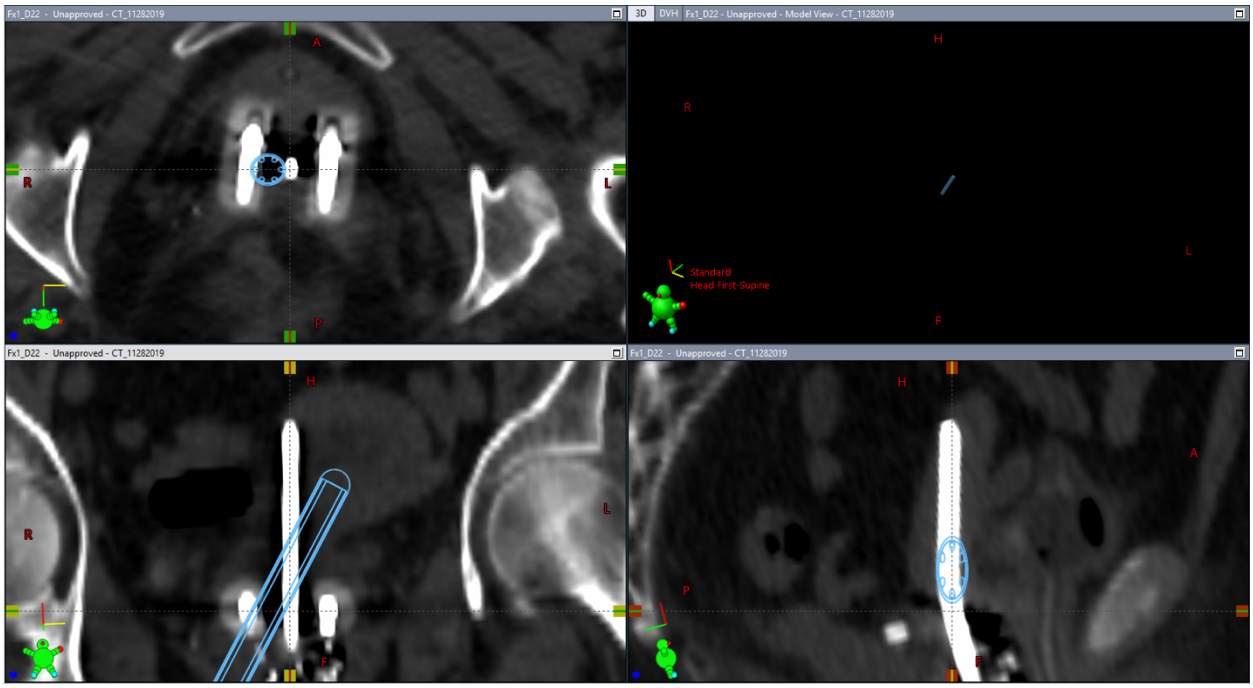

Figure 8. Digitized DMBT tandem unaligned with the original plan's conventional tandem.

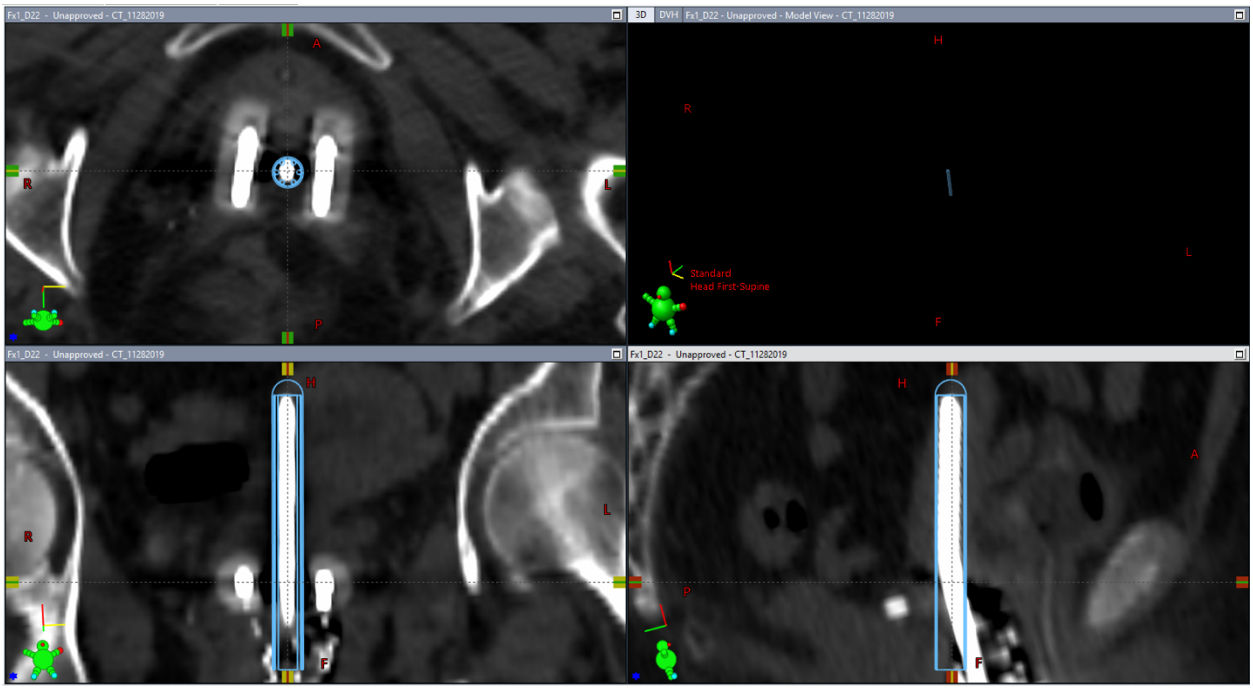

Figure 9. Digitized DMBT tandem aligned with the original plan's conventional tandem.

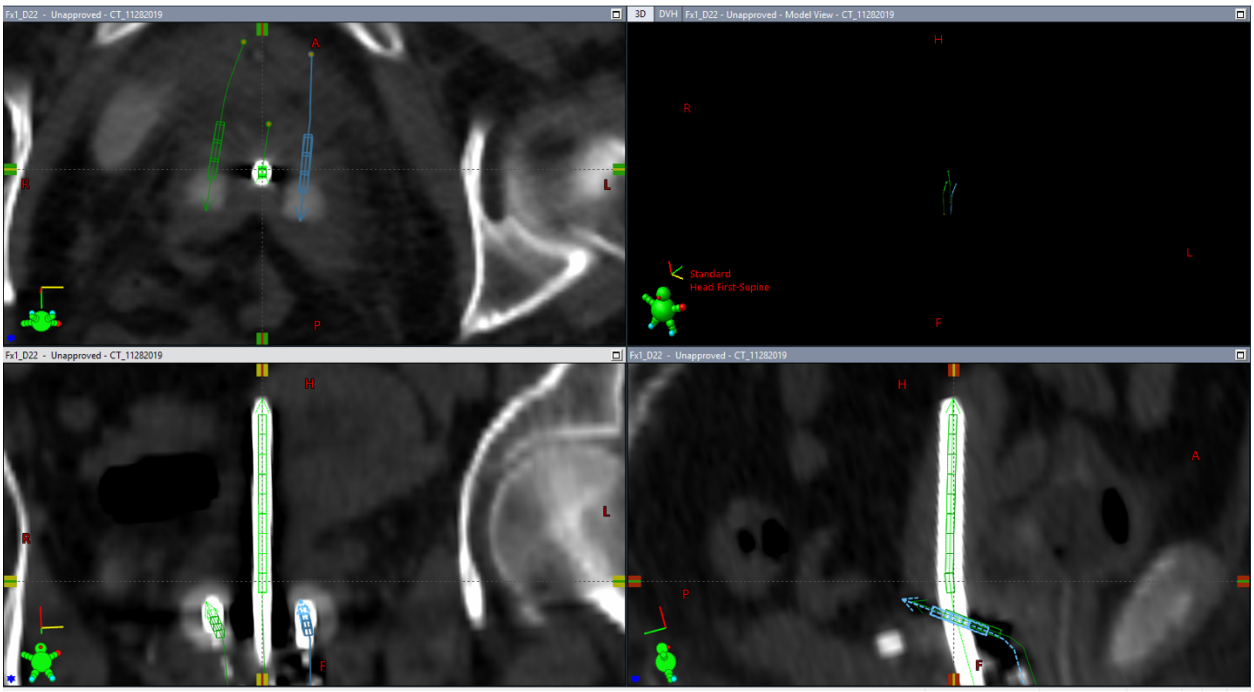

Figure 10. The original dwell positions used by the conventional tandem.

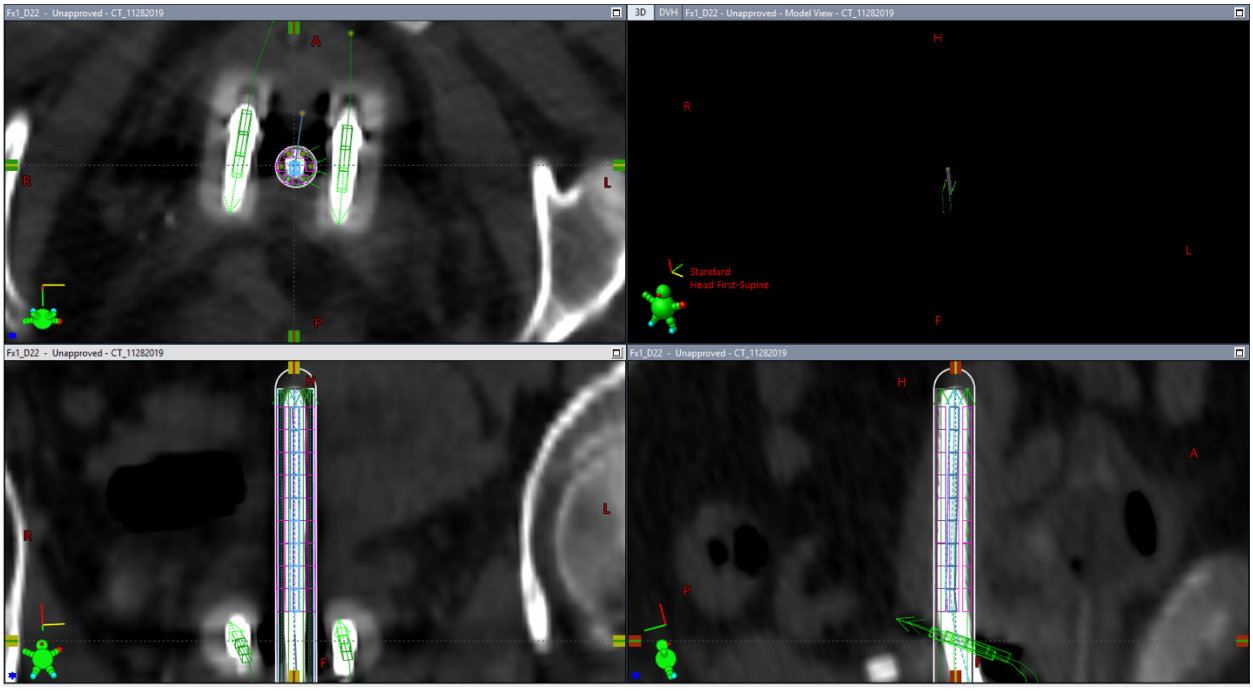

Figure 11. The new DMBT tandem's dwell positions are set to be equivalent to the dwell positions used by the original plan's conventional tandem. Blue rectangles indicate the dwell positions of the conventional tandem. Pink rectangles indicate the dwell positions of the DMBT tandem.

3.4.2. Reference Point Specification

Many cervical cancer survivors have incurred late-effects post treatment such as vaginal morbidity which can lead to sexual dysfunction [24-27]. The most abundant example is vaginal stenosis in which the vagina develops fibrous tissue due to radiation damage resulting in shortening of the vaginal canal [26,28]. Increasing vaginal doses will increase the likelihood of developing such late-effects. For this reason, we measured the dose to the vagina using a vaginal dose reporting method which accounts for the contributions from both external beam radiotherapy (EBRT) and brachytherapy (BT) [29]. In this method, reference points are set along the center of the vaginal canal in order to account for dose to the lower and middle portions of the vagina. To do this, a straight line is drawn from the posterior border of the symphysis bone (as identified on sagittal image slices) to the center of the tandem which acts as a surrogate for the center of the vaginal canal. The intersection of these two points is referred to the as the Posterior-Inferior Border of the Symphysis (PIBS) dose point. In order to set the PIBS reference points, a sagittal slice was selected in which the inferior most portion of the pubic symphysis bone was visible. The displayed view was rotated such that the horizontal dashed alignment lines were parallel with the bottom of the pubic symphysis bone. The vertical dashed alignment lines were then aligned along the center of the tandem which acted as a surrogate for the vaginal canal. The PIBS point was set at this location (see Figure 12). Additional PIBS points are measured at 1 cm and 2 cm superior and inferior to the PIBS points. To set these points, the measurement tool was used to measure 1 cm and 2 cm in the superior and inferior direction from the PIBS point

along a straight vertical path from the center of the tandem (see Figures 13-16). In addition , we sought to account for the dose to the upper vagina by measuring the dose to the ICRU's recto-vaginal reference point (RV-RP). According to the EMBRACE-1 study, a dose-effect relationship was created which related dose to the RV-RP to the likelihood of developing vaginal morbidity [29,30]. The RV-RP is defined as a point measured from the level of the superior end of the vaginal reference length (see Figure 17) to 5 mm laterally inwards of the rectum. The displayed view was rotated such that the horizontal dashed alignment lines could would be parallel with the junction of the tandem (the curve of the tandem) and passing through the rectum. The measurement tool within the TPS was used to measure 5 mm into the rectum along the dashed horizontal alignment line where the RV-RP was then set (see Figure 18).

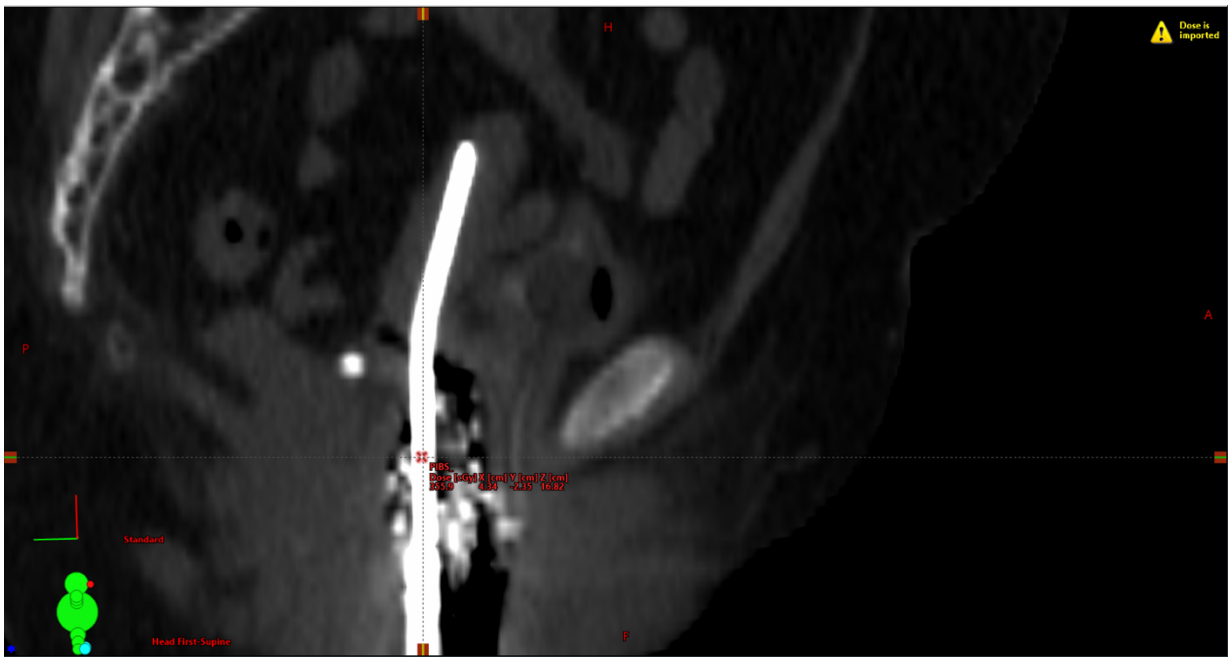

Figure 12 . Setting the PIBS point using the dashed horizontal alignment lines parallel with inferior border of the symphysis bone. The dashed vertical alignment lines were then set to the center of the tandem and were used as a guide for setting the remaining PIBS points.

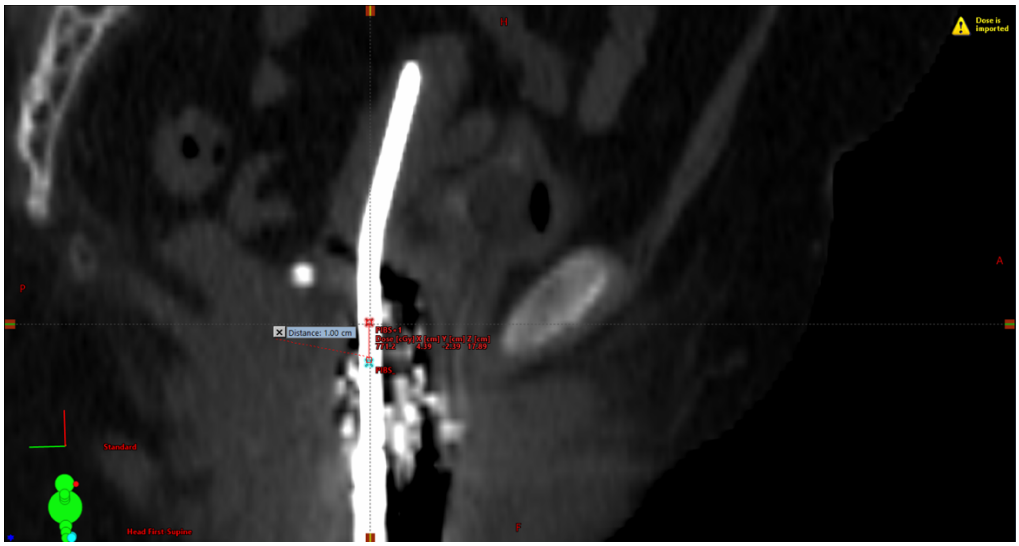

Figure 13. Setting the PIBS+1 point by measuring 1 cm superior from the PIBS point using the measurement tool and guided by the dashed vertical alignment line.

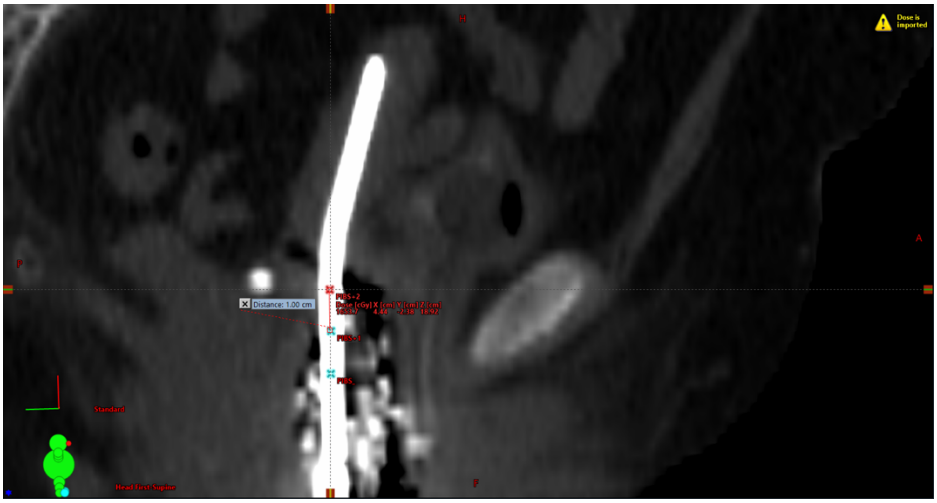

Figure 14. Setting the PIBS+2 point by measuring 1 cm superior from the PIBS+1 point using the measurement tool and guided by the dashed vertical alignment line.

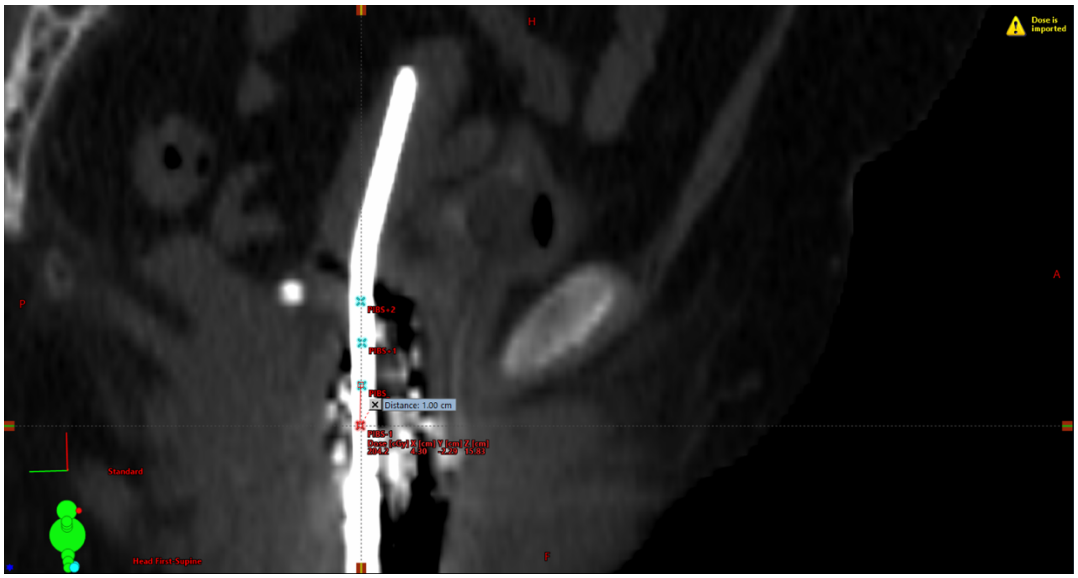

Figure 15. Setting the PIBS-1 point by measuring -1 cm inferior from the PIBS point using the measurement tool and guided by the dashed vertical alignment line.

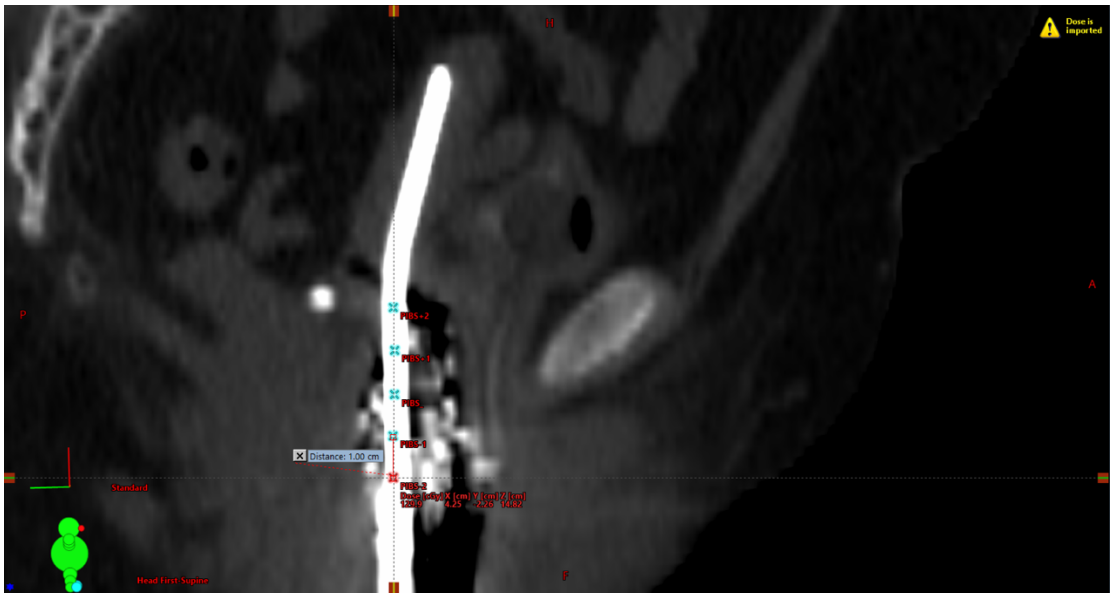

Figure 16. Setting the PIBS-2 point by measuring -1 cm inferior from the PIBS-1 point using the measurement tool and guided by the dashed vertical alignment line.

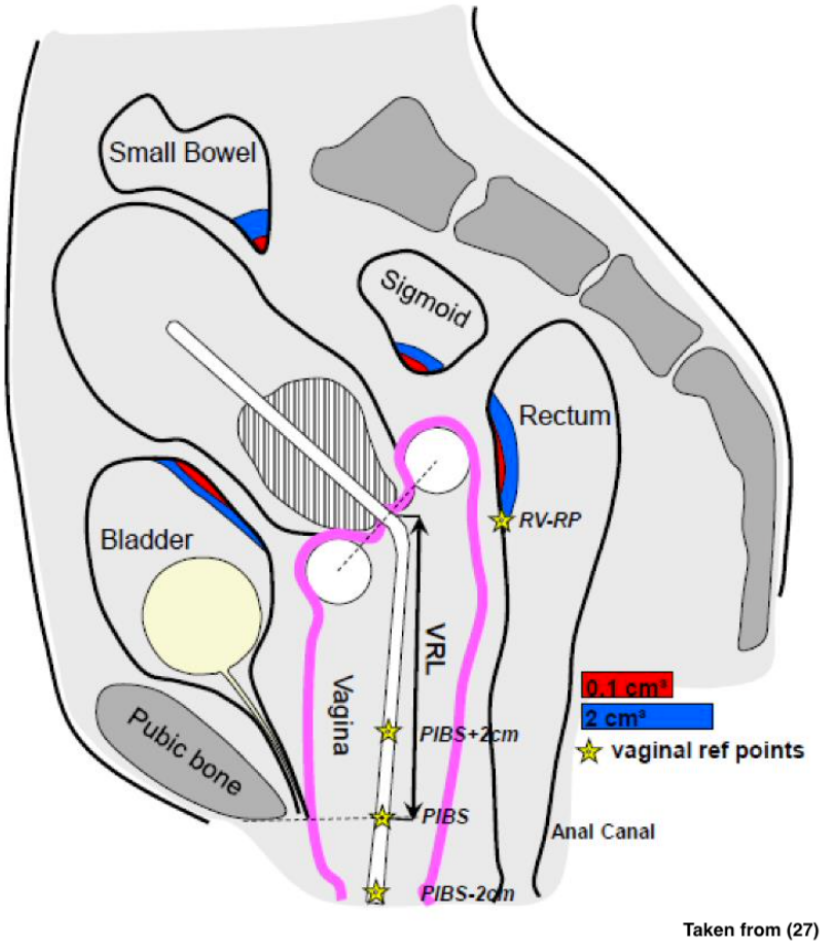

Figure 17. Definitions of the vaginal dose reference points (PIBS) and the ICRU's RV-RP

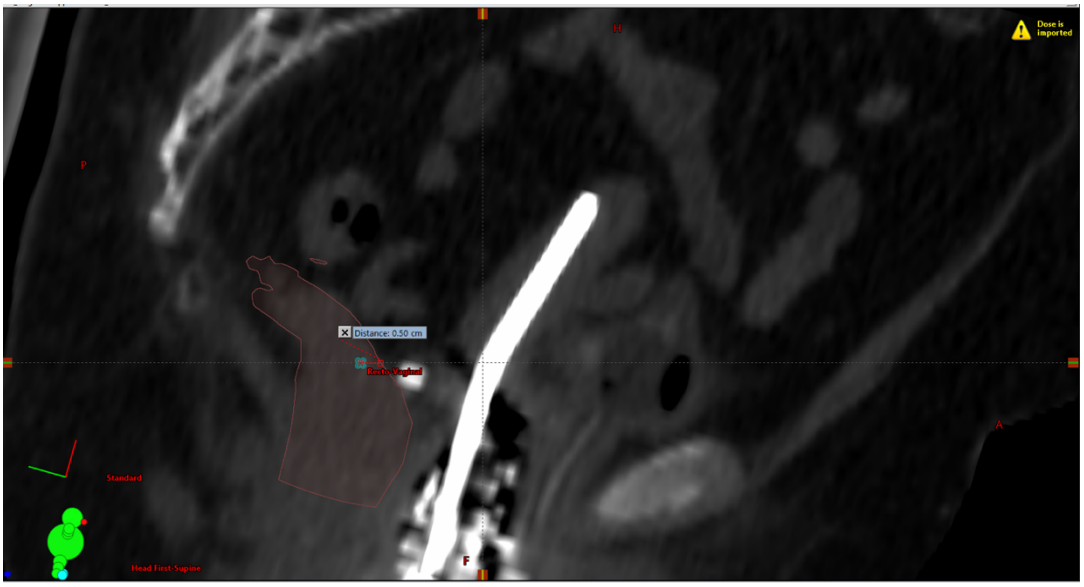

Figure 18. Setting the RV-RP using the dashed horizontal alignment lines parallel with the junction of the tandem. The measurement tool was then used to measure 5 mm into the rectum were the point was set.

3.4.3. Structure Generation

To ensure that the DMBT tandem's 100% isodose line retained the same shape as the original plan (pear-shape in the case of T&O plans), artificial contour structures were created. First, the 100% isodose line of the original plan was converted into a structure denoted as the "100% dose" structure (see Figure 19). Next, the *Contour* application was used to create two optimization structures. The first of which was the PTV which was created from subtracting areas of overlap between the OARs and the 100% dose structure while overlapping with the HRCTV (see Figures 20-21). This artificial PTV structure was used to maintain the shape of the 100% isodose line from the original plan. A second structure known as Optimization 2 (OPT2) was created to be a 3mm symmetric expansion about the PTV while excluding areas of overlap (see Figure 22). Thus OPT2 could be thought of as an outer rind or shell about the PTV and was used in order to confine the regions of high dose from extending into nearby OARs during the following optimization step.

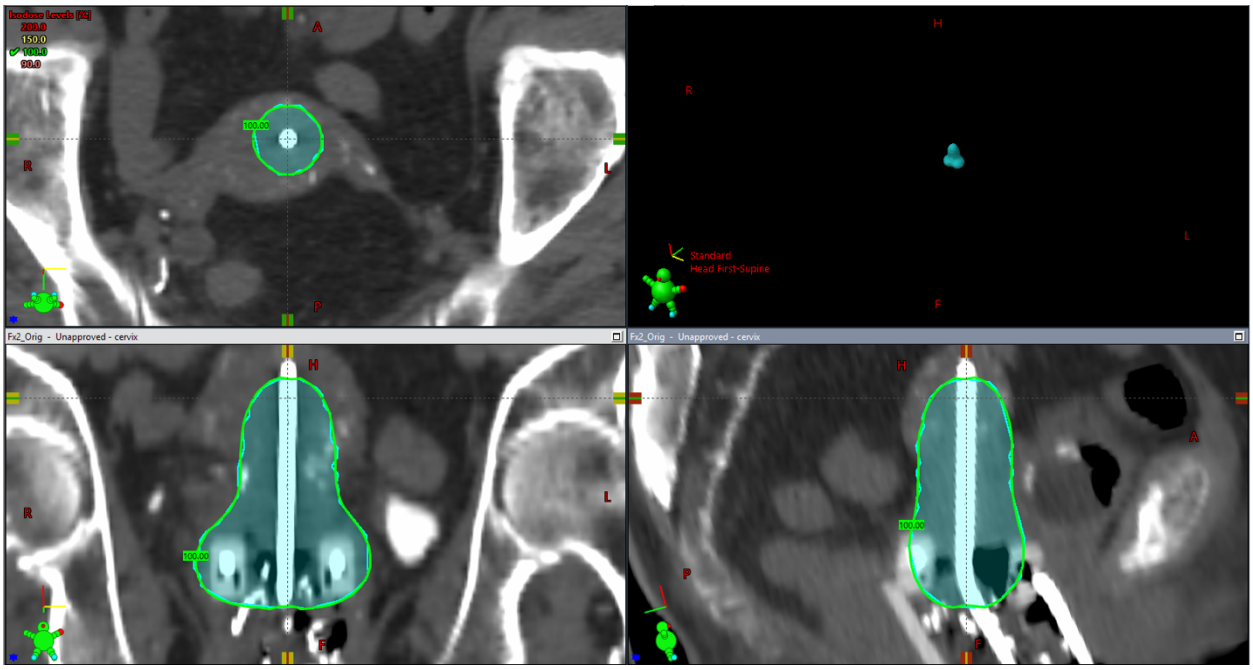

Figure 19. The 100% isodose structure (cyan) is created from the 100% isodose line (green) of the original plan and is used to subsequently contour the PTV and OPT2 structures.

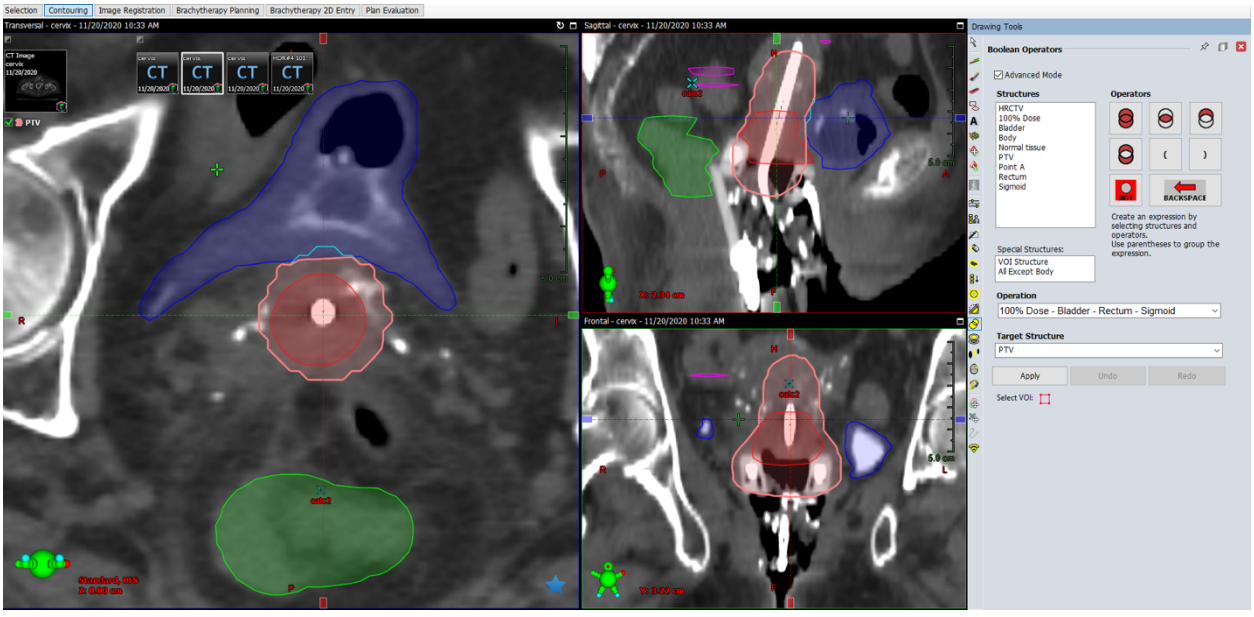

Figure 20. Creating the PTV. The first step was to create a structure that was equivalent to the 100% dose structure (cyan) excluding areas of overlap with the bladder (blue) , rectum (green), and sigmoid (magenta).

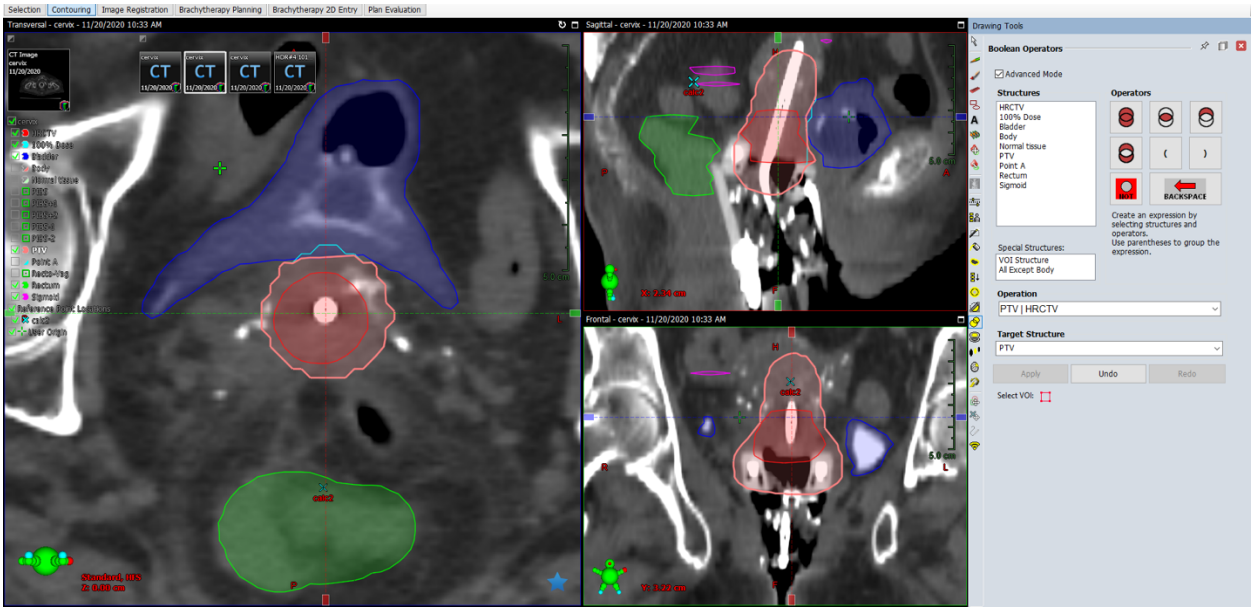

Figure 21. Creating the PTV (pink). The second step was to take the PTV structure created in Figure 20. and include areas missing the HRCTV (red). Note the extension of the PTV that now includes the HRCTV in the anterior direction. The PTV structure was created to maintain the shape of the original plan's 100% isodose line after optimization using the DMBT tandem model.

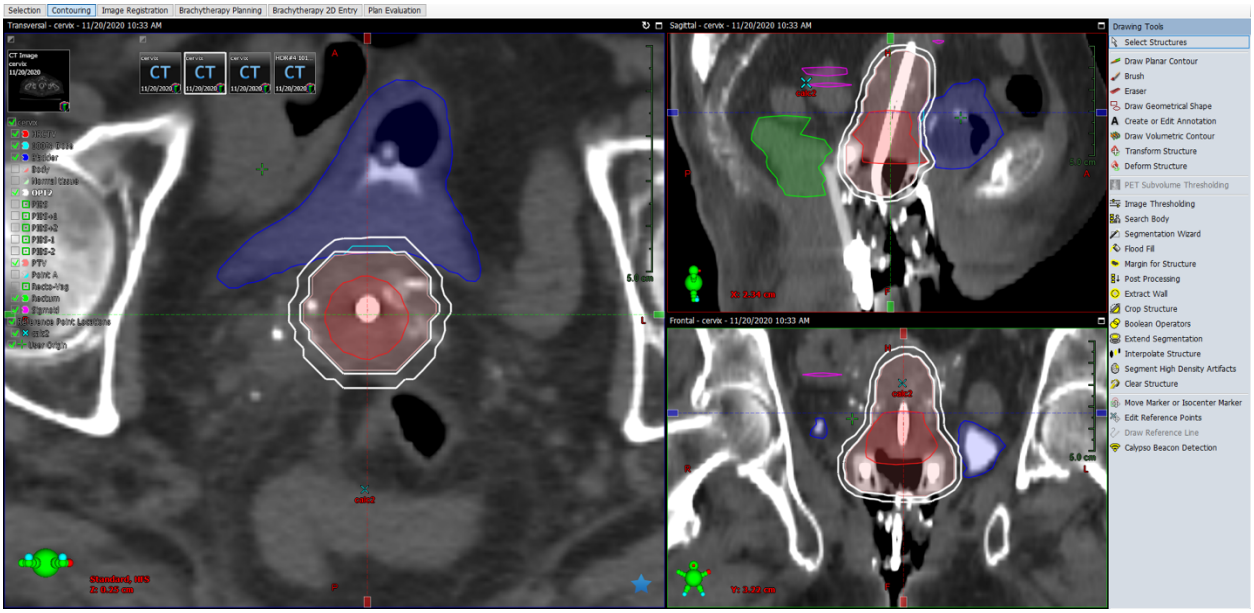

Figure 22. Creating the optimization 2 (OPT2) structure (white). A 3 mm symmetric outer margin was created from the PTV while excluding areas of overlap with the PTV. This created a rind or shell about the PTV. The OPT2 structure was used to confine areas of high dose from passing into nearby surrounding OAR during the optimization step.

3.4.4. Plan Optimization

Inverse optimization was performed using *VEGO Acuros BV Volume Optimization* in order to optimize and calculate the anisotropic Ir-192 doe distributions (see Figure 23). From this platform, the reporting medium was set to be equivalent to water. In this way, the tungsten-alloy heterogeneity of the DMBT tandem could be accounted for while minimizing the optimization time by treating all other heterogeneities including bone, soft tissue, and the ovoids or rings as water. This not only allows the heterogeneity of the DMBT tandem to be taken into account, but also provides a fair comparison to the original treatment plans which used TG-43 dose computation which considers a completely homogeneous water environment. Lower limit OAR dose constraints were represented by the D2cc and D1cc values of the original plan. Upper and lower HRCTV constraints were created in order to maintain the D90 value to within ± 1% of the original plan's D90. The artificially produced PTV structure was set such that at least 90% of its volume received at least 90% of the dose. This ensured that the new 100% isodose line would resemble the shape of the original plan's 100% isodose line. Lastly, the OPT2 constraint was set to receive no more than 100% of the dose to no more than $1cm^3$ of its volume ensuring that regions of high dose were prohibited from extending into the surrounding OAR (namely the bladder). The allowable violation of any OAR constraint was permitted to range from 1-10% while both the upper and lower limits on the HRCTV allowed no violation from the desired constraints ensuring strict obedience to the original plan's D90 value.

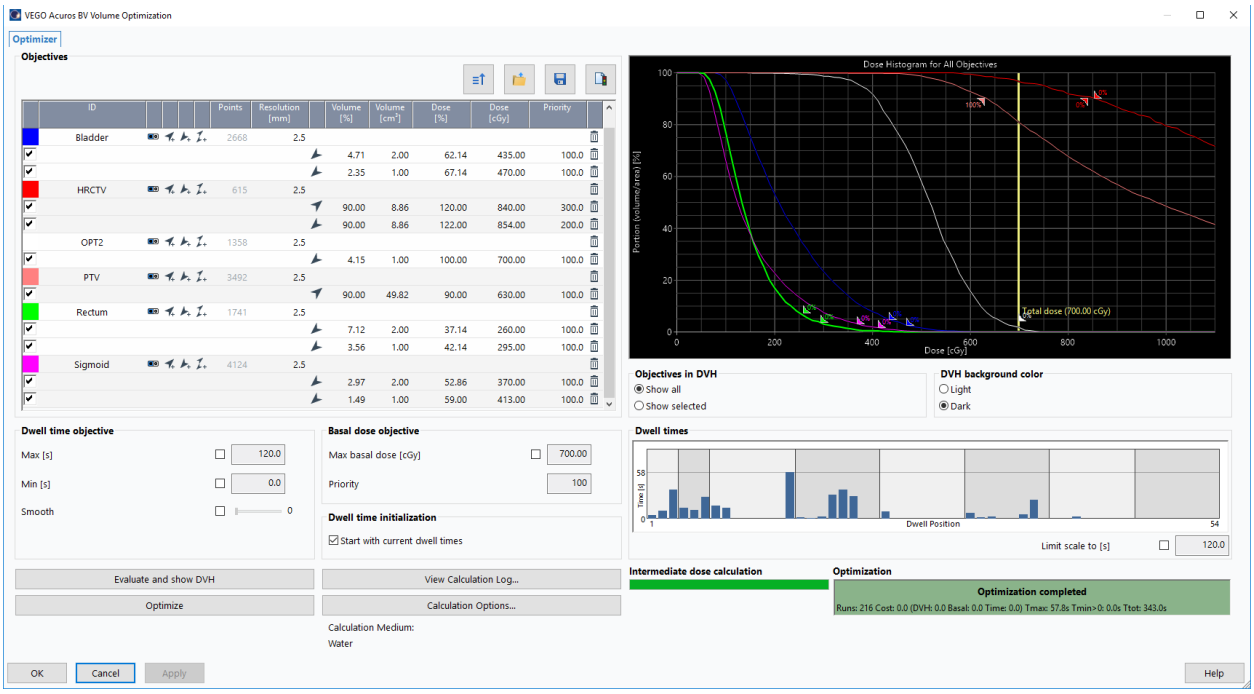

Figure 23. The optimization and calculation step used VEGO Acuros BV Volume optimization. The original plan's D2cc and D1cc OAR values were inputted as lower limits. The HRCTV constraints included and upper and lower constraint in order to ensure that the DMBT tandem plan's D90 value was maintained to within ±1% of the original plan's D90. An upper limit on the PTV was set to ensure that at least 90% of the volume received 90% of the dose. This ensured that the DMBT tandem plan's 100% isodose line closely resembled that of the original plan's. The lower limit set on the OPT2 constraint of no more than 1cc receiving no more than 100% of the dose ensures that regions of high dose are confined close to the DMBT tandem and to prevent hot spots in nearby OARs such as the bladder.

3.4.5. Data Collection

Upon successful completion of the optimization process, values from the new plan's DVH were recorded including the OAR D2cc and D1cc values and the HRCTV's D90 and V100 values. In addition, the dose to the RV-RP and all PIBS reference points were noted. The values of the original plan using the conventional tandem were then compared to the values of the new DMBT

tandem plan. Relative and absolute reductions in OAR doses were documented as well as the deviation in the new plan's D90 and V100 values from those of the original plan. The resulting plan was then compared to the original plan using the *plan evaluation* application in order to ensure that the shape of the original plan's 100% isodose line was retained.

3.5. Total Dose Calculation

The total biologic effective dose (EQD2) OAR D2cc values accounting for the contributions from external beam therapy and brachytherapy were calculated for all original and DMBT tandem plans and compared to those recommendations set by a 2021 ABS[34-39] review (see Figure 24) using the Withers formula (see Figure 25). The EBRT total dose was assumed to follow a common fractionation scheme of 45 Gy delivered over 25 fractions. The brachytherapy fractionization scheme was determined from the patient information provided that included the number of fractions and that the prescription dose per fraction . The modernly defined α/β value of 3 corresponding to the late-responding OARs were selected[43].

Quality measures and metrics for brachytherapy in cervical cancer

Quality Measures	Metrics	Level of Evidence	Source of Data
Multidisciplinary evaluation with a gynecologic oncologist, a surgical oncologist, medical oncologist, and/or radiation oncologist or discussion at a multi-disciplinary tumor board Use of brachytherapy in cervical cancer patients treated with primary radiation with curative intent in Stage I-IVA cervical cancer Coordination of care to complete radiation therapy within 8 weeks when possible/appropriate	D90 for HRCTV ≥ 85Gy[a] D 2cc of rectum < 65 Gy (maximum <75 Gy) D 2cc of bladder < 80 Gy (maximum <90 Gy) D 2cc of sigmoid < 70 Gy (maximum <75 Gy) Recto vaginal point <65 Gy (maximum 75 Gy)	**IC-IIA**	NCCN Guidelines (16) Viswanthan et al (17) Viswanthan et al (18) Lee et al (19) Serban et al (22) Potter et al (25)

Doses are in EQD2 combining EBRT plus brachytherapy dose.
[a] When meeting normal tissue constraints.

Figure 24. Total biologic effective dose (EQD2) limits (EBRT+BT) recommendations for the HRCTV and OAR in the treatment of cervical cancer from a recent 2021 ABS review article.

$$EQD_2 = D\left(\frac{d + \alpha/\beta}{2 + \alpha/\beta}\right)$$

Figure 25. The Withers formula used for calculating the total biologic effective dose (EQD2) to each OAR. "D" represents the total dose received over all fractions, "d' represents the dose per fraction, and the α/ β value was selected as 3 in accordance with the modernly accepted value for late-responding tissues.

3.6. Treatment Time Recording

Of additional concern was the amount of additional treatment time required with the use of the DMBT tandem. Because the activity of the source used varied amongst the original plans provided, we first had to scale the treatment times as if the 10 Ci source used by the DMBT tandem was utilized. In this way, the total treatment times between the original plans and the DMBT tandem plans could be compared fairly.

4. Results

4.1. Average Relative & Absolute OAR Dose Reduction

The D2cc values for each plan averaging the results from each of the 9 DMBT tandem models is presented in Table 3. The average relative reduction in the D2cc from using the DMBT tandem models for all patients were -11.00%, -21.76%, and -15.84% for the bladder, rectum, and sigmoid respectively. The maximum relative D2cc reductions achieved for a particular patient

from all DMBT tandem models was -16.28%, -52.13%, and -38.76% for the bladder, rectum, and sigmoid respectively.

		Bladder D2cc				Rectum D2cc				Sigmoid D2cc			
Patient no.	Fraction	Conv. (Gy)	DMBT (Gy)	Diff (Gy)	Diff (%)	Conv. (Gy)	DMBT (Gy)	Diff (Gy)	Diff (%)	Conv. (Gy)	DMBT (Gy)	Diff (Gy)	Diff (%)
1	1	4.15	3.68	0.47	-11.28%	3.07	2.62	0.45	-14.71%	2.92	2.42	0.51	-17.28%
2	1	4.32	4.03	0.29	-6.72%	3.81	3.18	0.62	-16.40%	3.53	2.96	0.57	-16.16%
3	1	5.30	4.89	0.41	-7.77%	2.56	1.83	0.73	-28.43%	5.14	4.53	0.61	-11.79%
4	1	4.03	3.51	0.52	-12.86%	3.69	3.38	0.31	-8.48%	3.59	3.37	0.22	-6.17%
5	1	2.70	2.44	0.26	-9.62%	3.67	3.52	0.16	-4.23%	1.56	1.27	0.30	-19.02%
6	1	5.23	4.51	0.71	-13.65%	3.35	1.60	1.75	-52.13%	3.64	2.23	1.41	-38.76%
	2	5.05	4.78	0.27	-5.35%	2.96	2.01	0.94	-31.91%	2.95	2.43	0.52	-17.54%
	3	5.15	4.33	0.82	-15.95%	3.40	2.49	0.91	-26.74%	4.49	3.72	0.77	-17.11%
7	1	6.20	5.55	0.65	-10.51%	2.47	1.96	0.52	-20.90%	4.07	3.45	0.62	-15.15%
	2	5.43	4.90	0.54	-9.86%	2.71	2.00	0.71	-26.26%	2.28	1.88	0.39	-17.35%
	3	5.80	4.88	0.92	-15.85%	2.97	2.77	0.20	-6.66%	1.82	1.32	0.50	-27.28%
	4	4.98	4.49	0.49	-9.87%	2.82	2.50	0.32	-11.27%	1.27	1.17	0.10	-7.64%
8	1	3.98	3.64	0.34	-8.57%	2.05	1.65	0.40	-19.46%	3.33	2.67	0.66	-19.89%
	2	4.55	4.12	0.42	-9.31%	1.18	0.86	0.32	-27.20%	2.14	1.78	0.36	-16.88%
	3	5.24	4.75	0.49	-9.43%	1.98	1.48	0.50	-25.47%	1.56	1.37	0.19	-12.22%
	4	4.79	4.24	0.55	-11.53%	3.01	2.25	0.76	-25.19%	3.41	3.00	0.41	-11.90%
9	1	5.11	4.61	0.51	-9.93%	2.72	2.31	0.40	-14.80%	3.18	2.90	0.27	-8.62%
	2	5.94	5.58	0.36	-6.12%	2.42	1.81	0.61	-25.25%	3.86	3.53	0.33	-8.46%
	3	5.19	4.59	0.60	-11.61%	2.48	1.60	0.88	-35.60%	3.62	3.11	0.51	-14.19%
10	1	5.55	4.69	0.86	-15.55%	4.02	3.17	0.85	-21.17%	2.97	2.30	0.67	-22.53%
11	1	6.11	5.47	0.64	-10.52%	3.74	3.27	0.47	-12.67%	3.53	2.96	0.57	-16.06%
	2	4.93	4.45	0.48	-9.66%	2.04	1.62	0.42	-20.43%	4.32	3.98	0.34	-7.86%
	3	4.66	3.90	0.76	-16.28%	3.83	3.24	0.59	-15.36%	2.03	1.63	0.40	-19.79%
12	1	5.60	4.69	0.91	-16.19%	1.93	1.32	0.61	-31.61%	3.74	3.35	0.39	-10.45%
	Average	5.00	4.45	0.55	-11.00%	2.87	2.27	0.60	-21.76%	3.12	2.64	0.48	-15.84%
	SD	0.78	0.70	0.20	0.03	0.73	0.74	0.33	0.11	1.01	0.93	0.26	0.07
	Minimum	2.70	2.44	0.26	-5.35%	1.18	0.86	0.16	-4.23%	1.27	1.17	0.10	-6.17%
	Maximum	6.20	5.58	0.92	-16.28%	4.02	3.52	1.75	-52.13%	5.14	4.53	1.41	-38.76%

Table 3 . D2cc values of each plan averaging the results from each of the 9 DMBT tandem models compared to the original plans.. Green shaded regions indicate areas of improvements over the original plan

The average relative reductions from each of the 9 DMBT tandem model averaged over all 24 plans are presented in Table 4 along with the average relative difference in D90 and V100 from the original plan. Note that the DMBT tandem plan's average D90 values varied no more than ±1% from the original plans indicating nearly identical HRCTV coverage. The average relative D2cc reductions from model 1 (thinnest model) were -9.65%, -19.91%, and -14.55% for the bladder, rectum, and sigmoid respectively. The average relative D2cc reductions from model 5 (moderate thickness) were -10.00%, -21.14%, and -15.61% for the bladder, rectum, and sigmoid respectively. The average relative D2cc reductions from model 9 (thickest model) were -12.82%, -24.69%, and -18.42% for the bladder, rectum, and sigmoid respectively. The difference in average relative D2cc reduction between the thickest (model 9) and the thinnest (model 1)

DMBT tandems models were 3.17%, 4.78 %, and 3.87 % for the bladder, rectum, and sigmoid respectively. It is worth noting that the relative D2cc reduction for the smallest target (HRCTV = 7.71 cm^3) averaging the results from all 9 DMBT tandem models were -13.65%, -52.13%, and -38.76% for the bladder, rectum, and sigmoid respectively. This corresponds to an absolute D2cc reduction of -0.71 Gy, -1.74 Gy, and -1.41 Gy for the bladder, rectum, and sigmoid respectively for the single fraction with a prescription dose of 7 Gy. The relative D2cc reduction for the largest target (HRCTV = 56.3 cm^3) averaging the results from all 9 DMBT tandem models were -10.82%, -14.71%, and -17.28% for the bladder, rectum, and sigmoid respectively. This corresponded to absolute D2cc reductions of -0.45 Gy, -0.45 Gy, and -0.51 Gy for the bladder, rectum, and sigmoid respectively for a single fraction with a prescription dose of 6 Gy. The maximum relative D2cc reduction for the bladder amongst all plans came from DMBT tandem model 3 and was -18.17% which corresponded to an absolute D2cc reduction of -1.05 Gy for a single fraction with a prescription dose of 7 Gy and a target volume of 15.74 cm^3. The maximum relative D2cc reduction for the rectum and sigmoid amongst all plans came from DMBT tandem model 9 (thickest) and was -72.51% and -47.21% respectively which corresponded to absolute D2cc reductions of -2.43 Gy and -1.72 Gy for a single fraction with a prescription dose of 7 Gy and a target volume of 7.71 cm^3 (smallest HRCTV).

Model	ΔV100 [%]	ΔD90 [%]	ΔD2cc Bladder [%]	ΔD1cc Bladder [%]	ΔD2cc Rectum [%]	ΔD1cc Rectum [%]	ΔD2cc Sigmoid [%]	ΔD1cc Sigmoid [%]
1 (t = 4 mm, $D_{channel}$ = 1.1mm)	-0.35%	0.21%	-9.65%	-9.19%	-19.91%	-20.51%	-14.55%	-14.39%
2 (t = 5 mm, $D_{channel}$= 1.1 mm)	-0.19%	0.31%	-10.51%	-10.32%	-20.58%	-21.16%	-14.41%	-14.31%
3 (t = 5 mm, $D_{channel}$= 1.3 mm)	-0.39%	0.05%	-10.63%	-10.25%	-21.84%	-22.46%	-15.70%	-15.64%
4 (t = 5.4 mm, $D_{channel}$= 1.1 mm)	-0.15%	0.38%	-10.57%	-10.51%	-21.07%	-21.70%	-14.73%	-14.66%
5 (t = 5.4 mm, $D_{channel}$= 1.3 mm)	-0.33%	0.22%	-10.00%	-9.73%	-21.14%	-21.82%	-15.61%	-15.59%
6 (t = 6 mm, $D_{channel}$= 1.1 mm)	-0.16%	0.35%	-11.57%	-11.62%	-21.82%	-22.97%	-16.35%	-16.32%
7 (t = 6 mm, $D_{channel}$= 1.3 mm)	-0.20%	0.27%	-10.88%	-10.86%	-21.88%	-22.50%	-15.88%	-15.82%
8 (t = 7 mm, $D_{channel}$= 1.3 mm)	-0.18%	0.30%	-12.18%	-12.36%	-22.93%	-23.50%	-16.89%	-16.80%
9 (t = 8 mm, $D_{channel}$= 1.3 mm)	0.05%	0.43%	-12.82%	-13.11%	-24.69%	-25.18%	-18.42%	-18.29%
Average	-0.21%	0.28%	-10.98%	-10.88%	-21.76%	-22.42%	-15.84%	-15.76%
SD	0.13%	0.11%	1.03%	1.26%	1.40%	1.38%	1.28%	1.28%
Minimum	0.05%	0.43%	-9.65%	-9.19%	-19.91%	-20.51%	-14.41%	-14.31%
Maximum	-0.39%	0.05%	-12.82%	-13.11%	-24.69%	-25.18%	-18.42%	-18.29%

Table 4. The average relative variance in the D90 [%] and V100 [100%] as well as the average relative reduction in the D2cc [%] and D1cc [%] of the bladder, rectum, and sigmoid for all 24 plans and for each of the 9 DMBT tandem models.

Figures 26-27 show the average relative reduction in D2cc from the 1.1 mm and 1.3 mm channel diameter DMBT tandem models respectively. Note the gradual improvement in relative D2cc reduction with increasing DMBT tandem thickness (increasing model number).

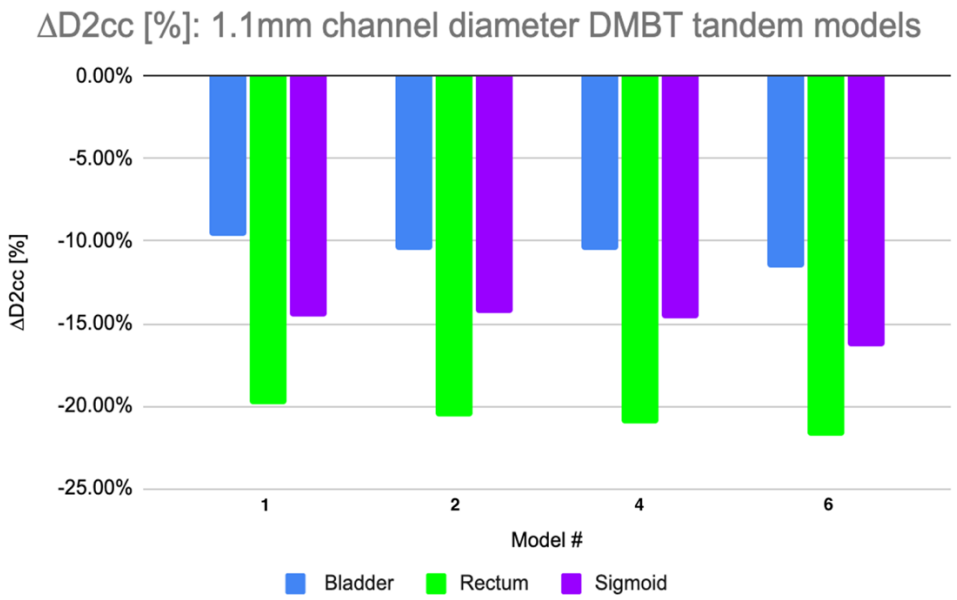

Figure 26. The average relative reduction in the D2cc of bladder, rectum, sigmoid for all 24 plans and for each of the 1.1mm channel diameter DMBT tandem models. Refer to fig. for DMBT tandem model details.

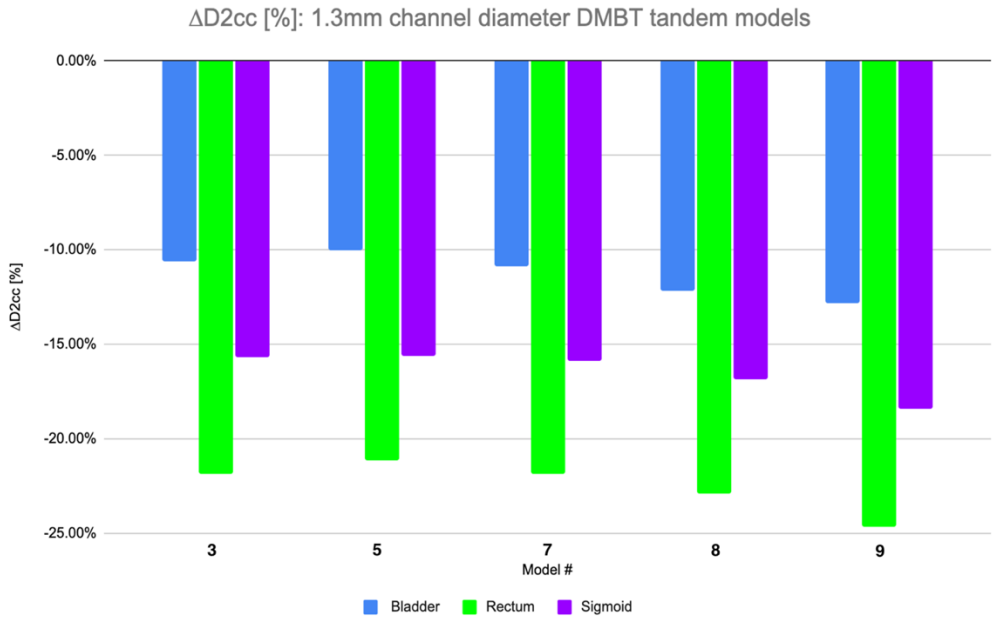

Figure 27. The average relative reduction in the D2cc of bladder, rectum, sigmoid for all 24 plans and for each of the 1.3mm channel diameter DMBT tandem models. Refer to fig. for DMBT tandem model details.

4.2. Target Size vs. Average Relative OAR Dose Reduction

The average relative D2cc reduction (%) for all plans is compared to HRCTV size (cm^3) for model 1 (thinnest), for model 5 (moderate thickness), and for model 9 (thickest) in Figure 28, Figure 29, and Figure 30 respectively.

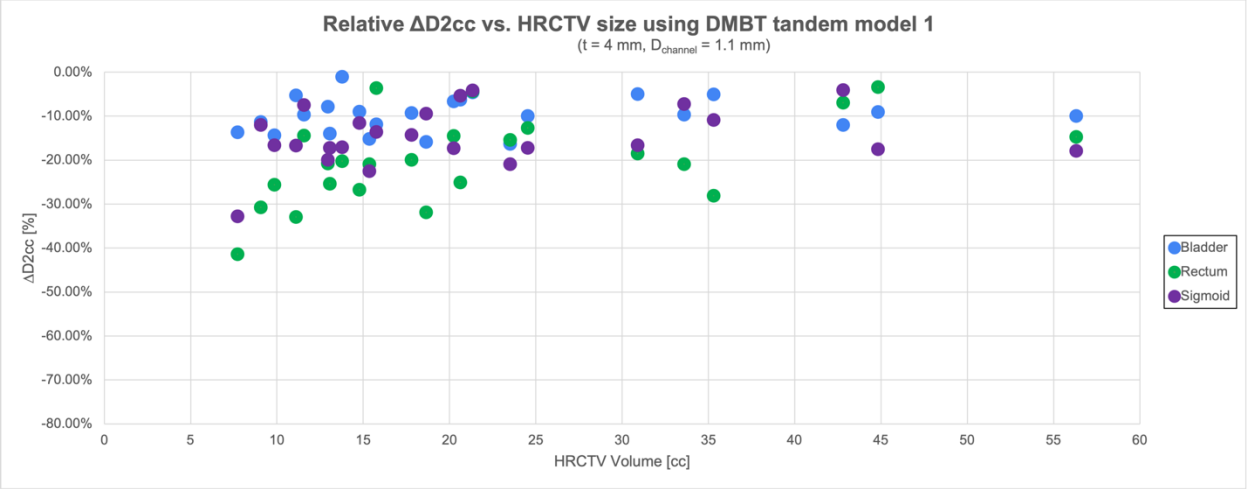

Figure 28. The relationship between HRCTV size (cc) and the average relative reduction in the D2cc of the bladder, rectum, and sigmoid for the thinnest DMBT tandem model (model 1).

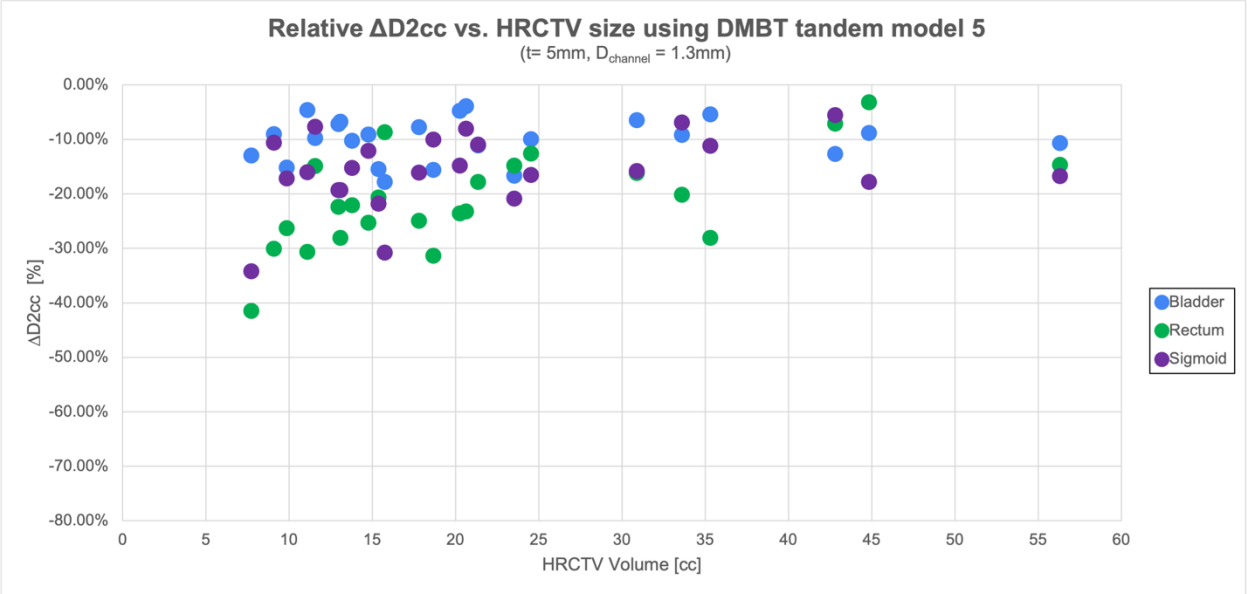

Figure 29. The relationship between HRCTV size (cc) and the average relative reduction in the D2cc of the bladder, rectum, and sigmoid for a moderate thickness DMBT tandem model (model 5).

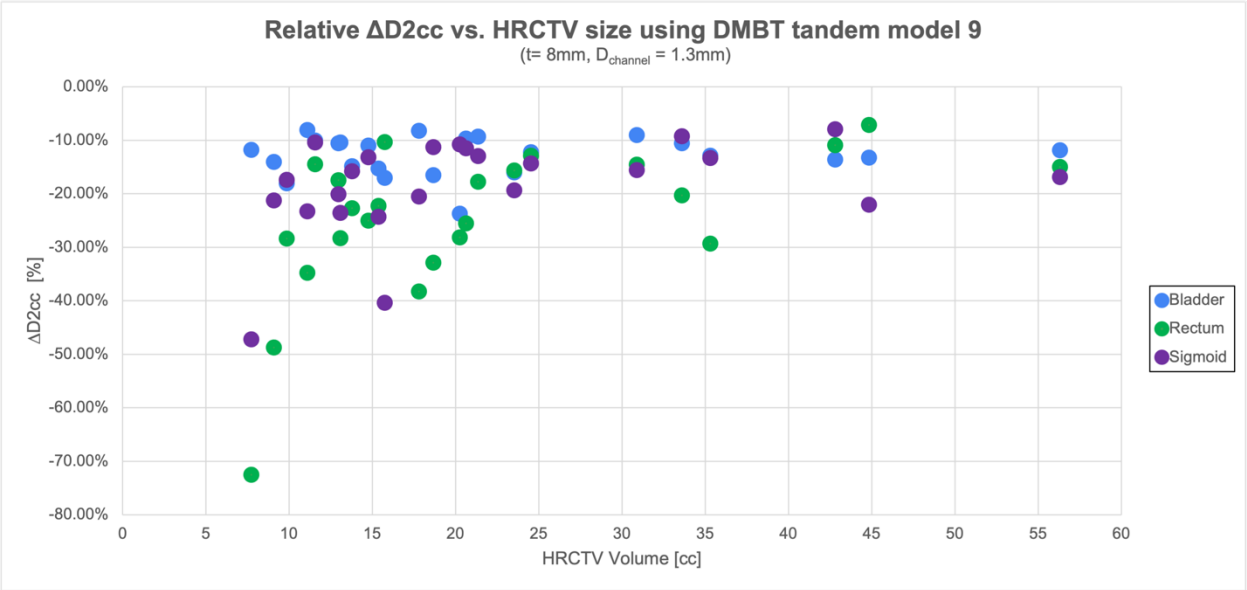

Figure 30. The relationship between HRCTV size (cc) and the average relative reduction in the D2cc of the bladder, rectum, and sigmoid for the thickest DMBT tandem model (model 9).

Figures 31-35 show the spatial dose distribution for various plans. Note the areas of improved OAR dose sparing.

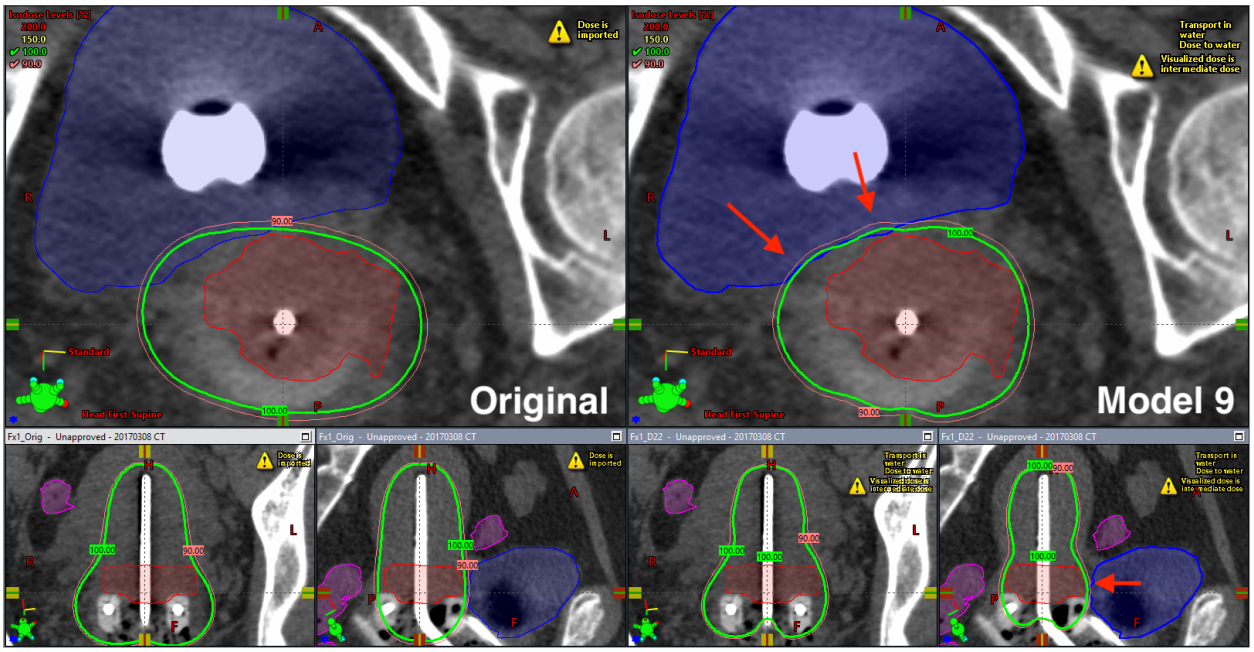

Figure 31. The spatial dose distribution of the original plan (left) and the DMBT tandem plan (right). The red arrows indicate areas of improved OAR sparing. This fraction belonged to patient 7 which had a HRCTV of 18.64 cm3 with a prescription dose of 6 Gy. The absolute reduction in OAR D2cc values from this model were -0.92 Gy, -0.63 Gy, and -0.42 Gy for the bladder, rectum and sigmoid respectively. Note the removal of the overlapping region of the 100% isodose line with the bladder when the DMBT tandem is used. Also note the retention of the pear-shape dose distributions with the DMBT tandem while generating significant improvements.

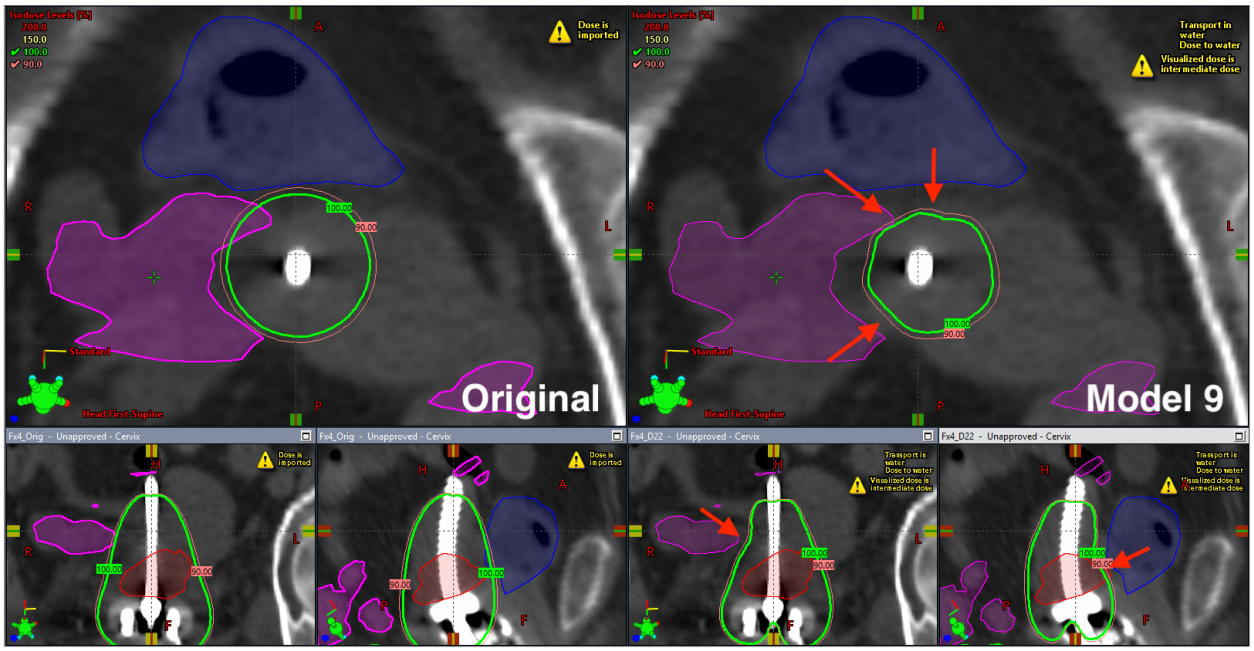

Figure 32. The spatial dose distribution of the original plan (left) and the DMBT tandem plan (right). The red arrows indicate areas of improved OAR sparing. This fraction belonged to patient 1 which had a HRCTV of 9.84 cm^3 with a prescription dose of 7 Gy. The absolute reduction in OAR D2cc values from this model were -0.93 Gy, -0.96 Gy, and -0.47 Gy for the bladder, rectum and sigmoid respectively. Note the removal of the overlapping region of the 100% isodose line with the sigmoid when the DMBT tandem is used.

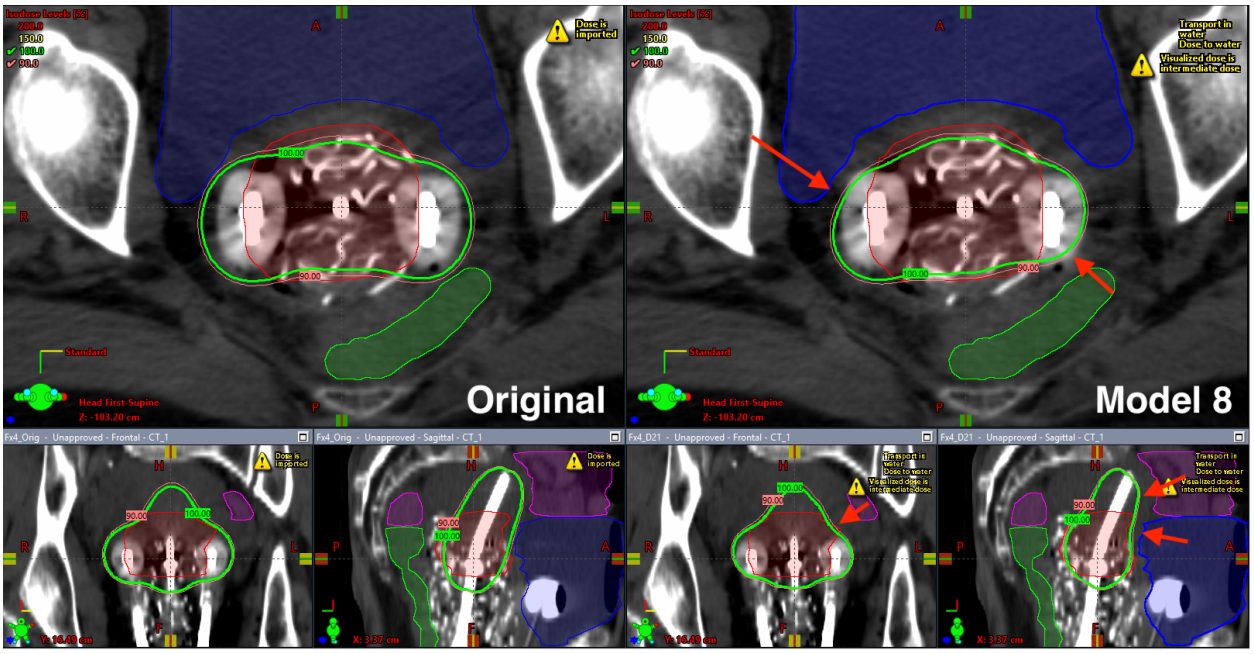

Figure 33. The spatial dose distribution of the original plan (left) and the DMBT tandem plan (right). The red arrows indicate areas of improved OAR sparing. This fraction belonged to patient 8 which had a HRCTV of 56.30 cm3 with a prescription dose of 6 Gy. The absolute reduction in OAR D2cc values from this model were -0.49 Gy, -0.46 Gy, and -0.49 Gy for the bladder, rectum and sigmoid respectively.

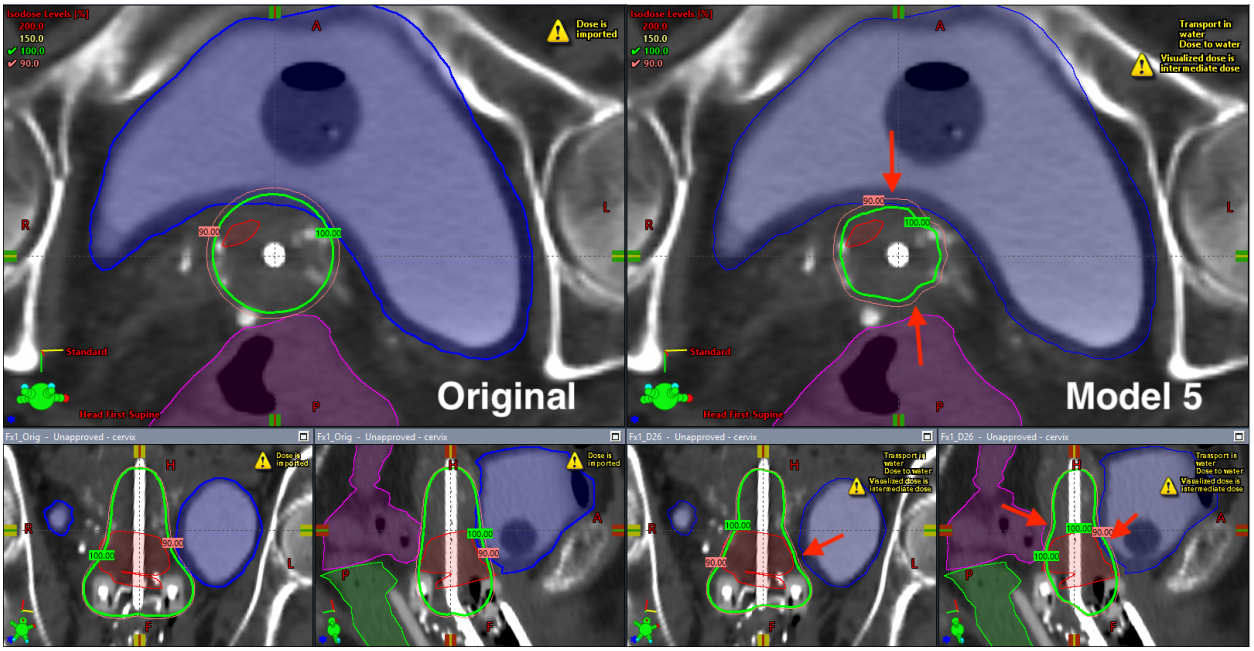

Figure 34. The spatial dose distribution of the original plan (left) and the DMBT tandem plan (right). The red arrows indicate areas of improved OAR sparing. This fraction belonged to patient 2 which had a HRCTV of 13.77 cm3 with a prescription dose of 7 Gy. The absolute reduction in OAR D2cc values from this model were -0.63 Gy, -0.55 Gy, and -0.62 Gy for the bladder, rectum and sigmoid respectively. Note the removal of the overlapping region of the 100% isodose line with the bladder when the DMBT tandem is used. Also note the retention of the pear-shape dose distribution with the DMBT tandem while generating significant improvements.

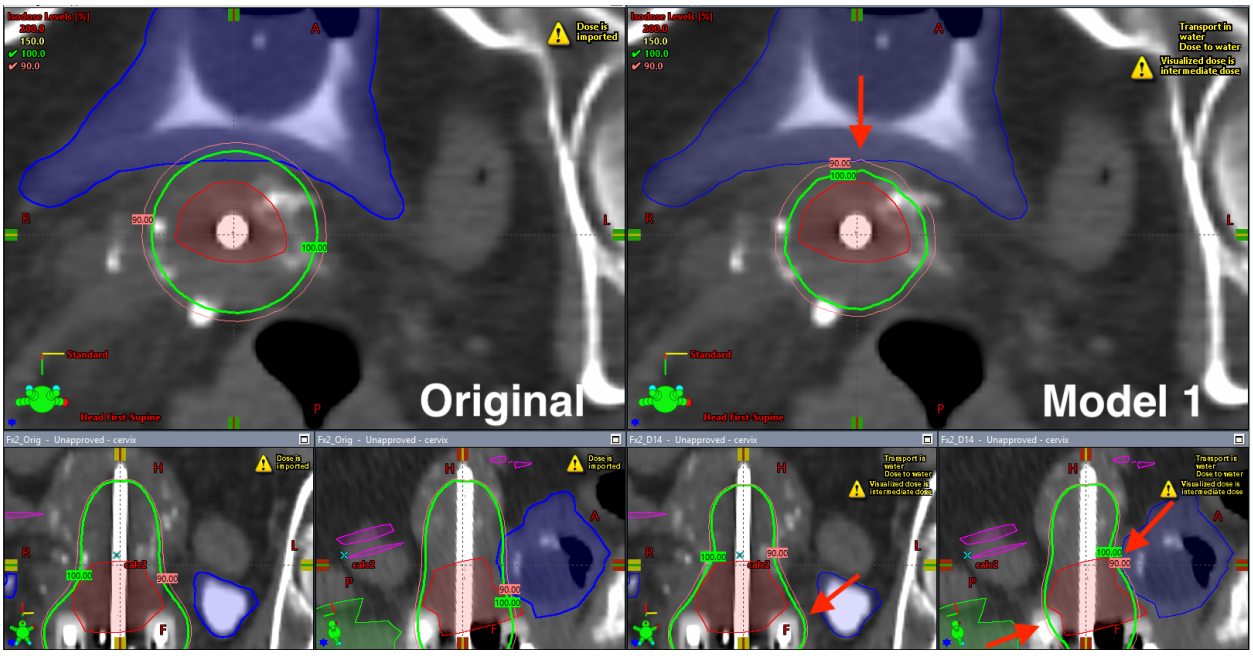

Figure 35. The spatial dose distribution of the original plan (left) and the DMBT tandem plan (right). The red arrows indicate areas of improved OAR sparing. This fraction belonged to patient 2 which had a HRCTV of 13.06 cm3 with a prescription dose of 7 Gy. The absolute reduction in OAR D2cc values from this model were -0.76 Gy, -0.69 Gy, and -0.39 Gy for the bladder, rectum and sigmoid respectively. Note the removal of the overlapping region of the 100% isodose line with the bladder when the DMBT tandem is used. Also note that model 1 is the weakest performing model and that significant improvements are made while maintaining the pear-shape dose distribution.

4.3. Total OAR Dose (EQD2) Reduction

The EQD2 D2cc values for each OAR and for each plan averaging the results of all 9 DMBT tandem models are presented in Table 5. The absolute EQD2 D2cc reductions averaged over all plans for all DMBT tandem model were -5.74 Gy, -4.02 Gy, -3.62 Gy for the bladder, rectum, and sigmoid respectively. The average absolute EQD2 D2cc reduction for model 1 (thinnest) were -3.60 Gy, -3.87 Gy, and -3.55 Gy for the bladder, rectum, and sigmoid respectively (see Figure 36). The average absolute EQD2 D2cc reduction for model 5 (moderate thickness) were -4.18 Gy, -4.18 Gy, and -3.74 Gy for the bladder, rectum, and sigmoid respectively (see Figure 37) . The average absolute EQD2 D2cc reduction for model 9 (thickest) were -4.05 Gy, -4.05 Gy, and -3.63 Gy for the bladder, rectum, and sigmoid respectively (see Figure 38). The difference in EQD2 D2cc reduction between the thickest (model 9) and the thinnest (model 1) DMBT tandems models were 0.45 Gy, 0.18 Gy, and 0.08 Gy for the bladder, rectum, and sigmoid respectively. 13 of the 24 original plans had at least one OAR failing its EQD2 D2cc dose limits. For 12 of those 13 plans, the addition of at least one of the 9 DMBT tandem models was able to lower the EQD2 D2cc for at least one OAR under its dose limit. Two notable plans that were reduced below their EQD2 D2cc limits are shown in Tables 7-8.

		Bladder EQD2 D2cc				Rectum EQD2 D2cc				Sigmoid EQD2 D2cc			
Patient no.	Fraction	Conv. (Gy)	DMBT (Gy)	Diff (Gy)	Diff (%)	Conv. (Gy)	DMBT (Gy)	Diff (Gy)	Diff (%)	Conv. (Gy)	DMBT (Gy)	Diff (Gy)	Diff (%)
1	1	72.91	67.84	5.07	-6.96%	61.84	57.91	3.92	-6.35%	60.52	56.30	4.21	-6.96%
2	1	81.09	77.15	3.94	-4.86%	74.27	66.80	7.47	-10.06%	70.83	64.35	6.49	-9.16%
3	1	78.36	74.04	4.32	-5.52%	54.59	50.28	4.30	-7.88%	76.63	70.49	6.14	-8.01%
4	1	77.20	70.64	6.56	-8.49%	72.85	69.07	3.78	-5.19%	71.58	68.94	2.64	-3.69%
5	1	58.63	56.51	2.12	-3.61%	67.71	66.13	1.58	-2.34%	50.34	48.60	1.73	-3.44%
6	1	77.58	70.32	7.26	-9.36%	60.23	49.23	11.01	-18.28%	62.55	52.56	10.00	-15.98%
	2	75.69	72.92	2.77	-3.66%	57.29	51.28	6.02	-10.50%	57.23	53.77	3.46	-6.05%
	3	76.82	68.61	8.21	-10.69%	60.63	54.15	6.47	-10.68%	70.11	63.22	6.89	-9.83%
7	1	88.80	81.17	7.63	-8.59%	54.03	50.96	3.07	-5.68%	66.22	61.03	5.19	-7.84%
	2	79.83	74.14	5.69	-7.13%	55.58	51.19	4.39	-7.89%	52.81	50.55	2.26	-4.28%
	3	84.02	73.98	10.04	-11.95%	57.36	55.98	1.37	-2.39%	50.23	47.82	2.41	-4.80%
	4	74.98	70.09	4.89	-6.52%	56.33	54.22	2.10	-3.73%	47.53	47.11	0.42	-0.88%
8	1	65.40	62.51	2.89	-4.43%	51.49	49.35	2.14	-4.15%	60.09	55.31	4.78	-7.95%
	2	70.64	66.70	3.95	-5.59%	47.15	45.86	1.29	-2.74%	52.01	50.01	2.00	-3.85%
	3	77.78	72.64	5.14	-6.61%	51.10	48.49	2.61	-5.10%	48.89	47.99	0.90	-1.85%
	4	73.10	67.82	5.28	-7.22%	57.64	52.66	4.99	-8.65%	60.68	57.64	3.04	-5.01%
9	1	68.10	64.22	3.87	-5.69%	52.51	50.58	1.94	-3.69%	54.96	53.47	1.49	-2.71%
	2	75.10	71.94	3.16	-4.21%	51.08	48.43	2.65	-5.20%	59.07	57.03	2.03	-3.44%
	3	68.73	64.11	4.62	-6.72%	51.36	47.62	3.74	-7.28%	57.60	54.60	2.99	-5.20%
10	1	81.17	72.03	9.14	-11.26%	65.79	58.85	6.94	-10.55%	57.37	52.95	4.42	-7.71%
11	1	87.74	80.24	7.50	-8.54%	63.40	59.60	3.80	-6.00%	61.60	57.31	4.29	-6.97%
	2	74.43	69.72	4.71	-6.33%	51.43	49.21	2.22	-4.32%	68.46	65.39	3.06	-4.48%
	3	71.78	64.76	7.02	-9.78%	64.09	59.36	4.73	-7.38%	51.38	49.24	2.14	-4.17%
12	1	91.34	79.29	12.05	-13.19%	52.74	48.92	3.83	-7.25%	68.36	64.43	3.94	-5.76%
	Average	76.30	70.56	5.74	-7.37%	58.02	54.01	4.02	-6.80%	59.88	56.25	3.62	-5.83%
	SD	7.45	5.86	2.47	0.03	7.14	6.44	2.29	0.04	8.14	6.91	2.18	0.03
	Minimum	58.63	56.51	2.12	-3.61%	47.15	45.86	1.29	-2.34%	47.53	47.11	0.42	-0.88%
	Maximum	91.34	81.17	12.05	-13.19%	74.27	69.07	11.01	-18.28%	76.63	70.49	10.00	-15.98%

Table 5. Individual EQD2 D2cc values, averaged over each patient's replanned fractions and all DMBT tandem models compared to the conventional (T&O and T&R) plans.

Model	ΔV100 [%]	ΔD90 [%]	ΔEQD2 D2cc Bladder [Gy]	ΔEQD2 D1cc Bladder [Gy]	ΔEQD2 D2cc Rectum [Gy]	ΔEQD2 D1cc Rectum [Gy]	ΔEQD2 D2cc Sigmoid [Gy]	ΔEQD2 D1cc Sigmoid [Gy]
1 (t = 4 mm, $D_{channel}$ = 1.1mm)	-0.35%	0.21%	-3.60	-5.97	-3.87	-4.82	-3.55	-4.24
2 (t = 5 mm, $D_{channel}$= 1.1 mm)	-0.19%	0.31%	-3.99	-6.68	-3.99	-4.96	-3.54	-4.28
3 (t = 5 mm, $D_{channel}$= 1.3 mm)	-0.39%	0.05%	-4.07	-6.82	-4.07	-5.03	-3.61	-4.37
4 (t = 5.4 mm, $D_{channel}$= 1.1 mm)	-0.15%	0.38%	-4.18	-7.52	-4.18	-5.27	-3.86	-4.67
5 (t = 5.4 mm, $D_{channel}$= 1.3 mm)	-0.33%	0.22%	-4.18	-7.04	-4.18	-5.19	-3.74	-4.52
6 (t = 6 mm, $D_{channel}$= 1.1 mm)	-0.16%	0.35%	-4.35	-7.97	-4.35	-5.39	-3.95	-4.78
7 (t = 6 mm, $D_{channel}$= 1.3 mm)	-0.20%	0.27%	-4.61	-8.39	-4.61	-5.69	-4.19	-5.09
8 (t = 7 mm, $D_{channel}$= 1.3 mm)	-0.18%	0.30%	-4.19	-6.72	-4.19	-5.22	-3.67	-4.44
9 (t = 8 mm, $D_{channel}$= 1.3 mm)	0.05%	0.43%	-4.05	-6.36	-4.05	-5.06	-3.63	-4.41
Average	-0.21%	0.28%	-4.14	-7.05	-4.17	-5.18	-3.75	-4.53
SD	0.13%	0.11%	0.27	0.77	0.22	0.26	0.22	0.27
Minimum	0.05%	0.43%	-3.60	-5.97	-3.87	-4.82	-3.54	-4.24
Maximum	-0.39%	0.05%	-4.61	-8.39	-4.61	-5.69	-4.19	-5.09

Table 6. The average relative variance in the D90 [%] and V100 [100%] as well as the average absolute reduction in the EQD2 D2cc [Gy] and EQD2 D1cc [Gy] of the bladder, rectum, and sigmoid for all 24 plans and for each of the 9 DMBT tandem models.

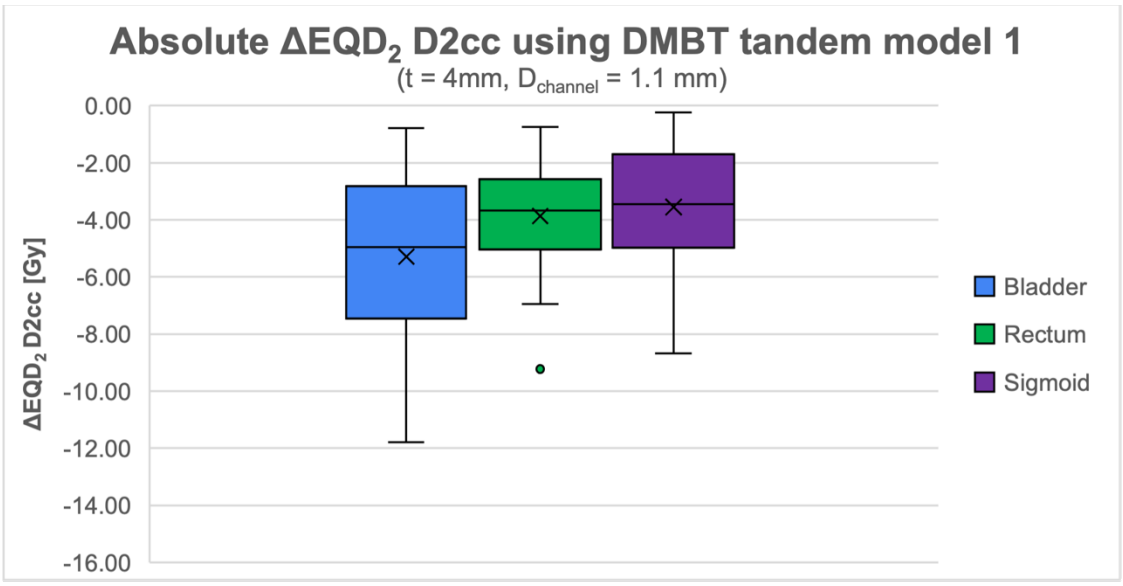

Figure 36. The average absolute reductions in EQD2 D2cc [Gy] averaged over all 24 plans for the bladder, rectum, and sigmoid for the thinnest DMBT tandem model (model 1). The top, middle, and bottom errors bars represent Q1, median, and Q3 respectively. The top and bottom whisker represents the minimum and maximum ΔEQD2 D2cc excluding outliers respectively. The "X" represents the average and the dots represent outliers.

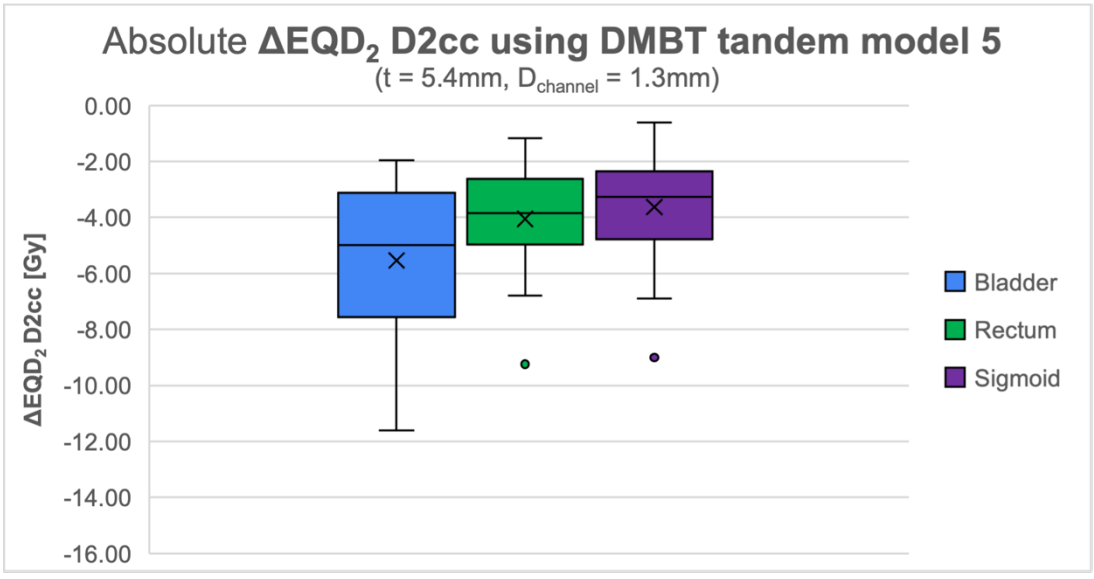

Figure 37. The average absolute reductions in EQD2 D2cc [Gy] averaged over all 24 plans for the bladder, rectum, and sigmoid for a moderately thick DMBT tandem model (model 5,). The top, middle, and bottom errors bars

represent Q1, median, and Q3 respectively. The top and bottom whisker represents the minimum and maximum ΔEQD2 D2cc excluding outliers respectively. The "X" represents the average and the dots represent outliers.

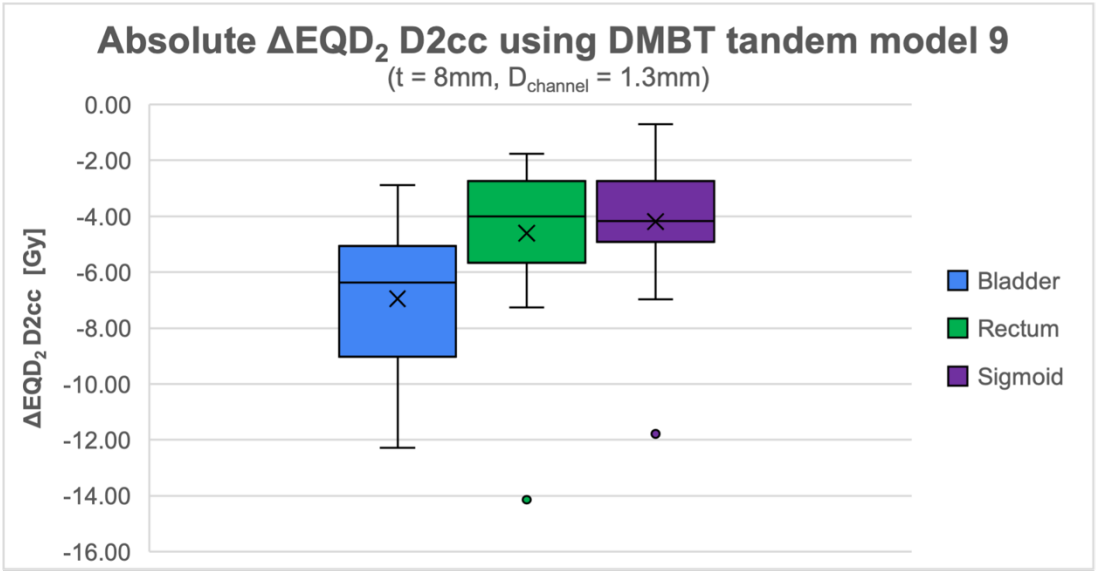

Figure 38. The average absolute reductions in EQD2 D2cc [Gy] averaged over all 24 plans for the bladder, rectum, and sigmoid for the thickest DMBT tandem model (model 9). The top, middle, and bottom errors bars represent Q1, median, and Q3 respectively. The top and bottom whisker represents the minimum and maximum ΔEQD2 D2cc excluding outliers respectively. The "X" represents the average and the dots represent outliers.

Patient 7: Plan 1	ΔV100 [%]	ΔD90 [%]	ΔEQD2 D2cc Bladder [Gy]	ΔEQD2 D1cc Bladder [Gy]	ΔEQD2 D2cc Rectum [Gy]	ΔEQD2 D1cc Rectum [Gy]	ΔEQD2 D2cc Sigmoid [Gy]	ΔEQD2 D1cc Sigmoid [Gy]
Original Plan	**99.68**	**120.68**	**91.34**	**100.95**	**52.74**	**54.06**	68.36	71.33
1 (t = 4 mm, $D_{channel}$ = 1.1mm)	98.67	120.52	79.56	84.92	48.89	49.60	64.80	67.14
2 (t = 5 mm, $D_{channel}$= 1.1 mm)	98.74	119.51	79.47	84.64	48.95	49.65	64.45	66.74
3 (t = 5 mm, $D_{channel}$= 1.3 mm)	98.84	120.05	79.79	85.03	49.01	49.72	64.91	67.26
4 (t = 5.4 mm, $D_{channel}$= 1.1 mm)	99.07	120.82	79.31	84.46	48.93	49.63	64.36	66.57
5 (t = 5.4 mm, $D_{channel}$= 1.3 mm)	98.82	119.71	79.72	84.92	48.95	49.66	64.59	66.83
6 (t = 6 mm, $D_{channel}$= 1.1 mm)	99.10	120.82	79.08	84.08	48.91	49.61	64.29	66.47
7 (t = 6 mm, $D_{channel}$= 1.3 mm)	98.96	120.32	79.25	84.42	48.91	49.61	64.26	66.49
8 (t = 7 mm, $D_{channel}$= 1.3 mm)	99.40	120.37	78.40	83.26	48.91	49.62	64.06	66.15
9 (t = 8 mm, $D_{channel}$= 1.3 mm)	99.71	121.23	79.06	84.13	48.78	49.48	64.12	66.20

Table 7. The absolute difference in total dose (EQD2) between a single plan from patient 7 and the DMBT plans. Note the significant reduction in EQD2 D2cc for the bladder which was originally exceeding its total dose (EQD2) limit of 80 Gy (red shaded region) using all DMBT tandem models (green shaded region).

Patient 5: Plan 1	ΔV100 [%]	ΔD90 [%]	ΔEQD2 D2cc Bladder [Gy]	ΔEQD2 D1cc Bladder [Gy]	ΔEQD2 D2cc Rectum [Gy]	ΔEQD2 D1cc Rectum [Gy]	ΔEQD2 D2cc Sigmoid [Gy]	ΔEQD2 D1cc Sigmoid [Gy]
Original Plan	**89.87**	**99.74**	**81.17**	**92.12**	**65.79**	**71.57**	57.37	60.20
1 (t = 4 mm, $D_{channel}$ = 1.1mm)	89.59	99.33	72.25	78.84	58.94	61.83	52.96	54.72
2 (t = 5 mm, $D_{channel}$= 1.1 mm)	90.63	100.85	72.36	78.84	59.00	62.03	53.10	54.87
3 (t = 5 mm, $D_{channel}$= 1.3 mm)	90.00	100.00	72.58	79.10	58.94	61.88	53.23	55.03
4 (t = 5.4 mm, $D_{channel}$= 1.1 mm)	90.62	100.97	72.02	78.20	58.97	62.02	53.04	54.83
5 (t = 5.4 mm, $D_{channel}$= 1.3 mm)	89.91	99.84	72.09	78.45	59.01	61.97	53.08	54.84
6 (t = 6 mm, $D_{channel}$= 1.1 mm)	89.98	99.97	71.59	77.49	58.80	61.78	52.77	54.52
7 (t = 6 mm, $D_{channel}$= 1.3 mm)	90.47	100.84	71.85	78.03	58.98	62.00	52.92	54.66
8 (t = 7 mm, $D_{channel}$= 1.3 mm)	89.95	99.91	71.32	76.78	58.50	61.45	52.80	54.51
9 (t = 8 mm, $D_{channel}$= 1.3 mm)	91.01	101.59	72.21	77.68	58.54	61.53	52.63	54.31

Table 8. The absolute difference in total dose (EQD2) between a single plan from patient 5 and the DMBT plans. Note the significant reduction in EQD2 D2cc for the bladder and rectum which were originally exceeding its total dose (EQD2) limits (red shaded region) of 80 Gy and 65 Gy respectively using all DMBT tandem models (green shaded region).

4.4. Average Relative RV-RP & PIBS Dose Reductions

The average relative reduction by all 9 DMBT tandem models was -21.87%, -27.90%, -21.19%, -17.97%, and -17.35% for the RV-RP, PIBS+2, PIBS+1, PIBS, PIBS-1, and PIBS-2 respectively (see Table 9). The minimum relative reductions came from model 1 (thinnest) and were -19.30%, -21.55%, -16.30%, -13.99%, -14.50%, and -13.73% for the RV-RP point, PIBS+2, PIBS+1, PIBS, PIBS-1, and PIBS-2 respectively. The maximum relative reductions came from

model 9 (thickest) and were -26.49%, -37.84%, -29.99%, -25.75%, -22.45%, and -21.74% for the RV-RP, PIBS+2, PIBS+1, PIBS, PIBS-1, and PIBS-2 respectively.

Model	ΔRecto-Vaginal point [%]	ΔPIBS+2cm [%]	ΔPIBS+1 cm [%]	ΔPIBS [%]	ΔPIBS-1cm [%]	ΔPIBS-2cm [%]
1 (t = 4 mm, $D_{channel}$ = 1.1mm)	-19.30%	-21.55%	-16.30%	-13.99%	-14.50%	-13.73%
2 (t = 5 mm, $D_{channel}$= 1.1 mm)	-19.96%	-23.67%	-22.20%	-17.77%	-16.73%	-15.94%
3 (t = 5 mm, $D_{channel}$= 1.3 mm)	-20.56%	-27.71%	-18.50%	-17.78%	-17.56%	-16.68%
4 (t = 5.4 mm, $D_{channel}$= 1.1 mm)	-21.00%	-25.55%	-22.32%	-18.24%	-16.92%	-16.21%
5 (t = 5.4 mm, $D_{channel}$= 1.3 mm)	-21.01%	-25.70%	-17.78%	-16.98%	-16.64%	-16.12%
6 (t = 6 mm, $D_{channel}$= 1.1 mm)	-22.26%	-28.13%	-19.23%	-18.24%	-17.82%	-17.42%
7 (t = 6 mm, $D_{channel}$= 1.3 mm)	-22.34%	-27.74%	-19.43%	-18.80%	-18.33%	-18.05%
8 (t = 7 mm, $D_{channel}$= 1.3 mm)	-23.94%	-33.19%	-24.97%	-22.12%	-20.78%	-20.30%
9 (t = 8 mm, $D_{channel}$= 1.3 mm)	-26.49%	-37.84%	-29.99%	-25.75%	-22.45%	-21.74%
Average	-21.87%	-27.90%	-21.19%	-18.85%	-17.97%	-17.35%
SD	2.22%	4.94%	4.24%	3.33%	2.36%	2.42%
Minimum	-19.30%	-21.55%	-16.30%	-13.99%	-14.50%	-13.73%
Maximum	-26.49%	-37.84%	-29.99%	-25.75%	-22.45%	-21.74%

Table 9. The average relative reduction in the dose to the RV-RP (%) and PIBS points (%) for all 24 plans and for each of the 9 DMBT tandem models.

4.5. Treatment Time

The average increase in the total treatment time relative to the original treatment plan times are shown in Table 10. Note that the total treatment time increases with increasing model number/DMBT tandem thickness. The average total treatment time of all 24 original plans was 307.85 s (5.13 min.). The minimum and maximum average total treatment times produced by the DMBT tandems were 324.19 s (5.4 min.) and 394.48 s (6.57 min.) respectively.

Model	Average Original Total Treatment Time (s)	Average DMBT Total Treatment Time (s)	ΔTotal Treamtent Time (s)
#1 (t=4mm, Dchannel=1.1mm)	307.85	324.19	16.33
#2 (t=5mm, Dchannel=1.1mm)		345.75	37.9
#3 (t=5mm, Dchannel=1.3mm)		334.83	26.98
#4 (t=5.4mm, Dchannel=1.1mm)		354.73	46.88
#5 (t=5.4mm, Dchannel=1.3mm)		343.6	35.75
#6 (t=6mm, Dchannel=1.1mm)		362.93	55.08
#7 (t=6mm, Dchannel=1.3mm)		359.57	51.71
#8 (t=7mm, Dchannel=1.3mm)		377.68	69.82
#9 (t=8mm, Dchannel=1.3mm)		394.48	86.63
	Mean	355.31	47.45
	SD	21.59	21.59

Table 10. The average treatment time of all original plans and all DMBT tandem plans for each of the 9 models as well as the average increase in the total treatment time

5. Discussion

The results in Table 4 represent a general improvement of using all DMBT tandem models. One may note that the smallest and greatest reduction in OAR dose with the aid of all DMBT tandem models were to the bladder and rectum respectively. This may be explained by the close proximity of the bladder to the tandem relative to the distant rectum. It is apparent that the thickest DMBT tandem (model 9) reduced OAR doses to the bladder, rectum, and sigmoid by the greatest amount relative to the other models. This is likely due to the increase thickness of the tungsten-alloy which is used to attenuate backside radiation. On the contrary, the smallest reduction in OAR doses to the bladder, rectum, and sigmoid came from the thinnest DMBT tandem (model 1) and can likely be explained by the same principle. In general, as the DMBT tandem thickness increases so does the relative reduction in OAR doses (see Figures 26-27). Despite a 4 mm difference in thickness between the thickest (model 9) and thinnest (model 1) DMBT tandem models, the difference in OAR dose reductions were minimal. It would appear that only marginal improvements are achieved by the thicker DMBT tandem models; however, these small differences may be considerable when straddling total dose (EQD2) limits for a particular OAR. From the results, it may seem apparent that the thickest DMBT tandem (model 9) should be used; however, due to the small diameter of the cervical os, it becomes increasingly difficult for correct applicator placement by the physician as the tandem thickness increases. Model 5 was identified to be a potentially useful applicator in the clinical setting as its thickness (5.4 mm) closely resembles that of conventional tandem used currently (3-6 mm). In addition, the difference in OAR dose reductions between the moderately thick (model 5) and thickest

(model 9) DMBT tandem models were marginal. This small deficit in performance for a moderately thick (model 5) DMBT tandem may be a reasonable clinical compromise for better ease and accuracy of placement. An additional consideration was the target size. It was observed that the reduction in dose to the OAR decreased as HRCTV size increased. This was to be expected as dose modulation decreases with increasing distance from the tandem (especially beyond 2-3 cm from the DMBT tandem) due to the inverse square law. In addition, larger targets may be closer to OARs and thus it becomes increasingly difficult to maintain sufficient target coverage without depositing additional dose in those structures. Despite this, all plans regardless of target size experienced significant reductions in OAR dose. Improvements were seen from our plan with smallest (HRCTV = 7.71cm^3) through the largest target (HRCTV = 56.3 cm^3) plan. In no plan for any DMBT tandem model did the new OAR dose values exceed the original plan's values. There was always improvement. The largest improvements in OAR dose reduction for the sigmoid and rectum came from the smallest target (HRCTV = 7.71cm^3). The largest relative improvement in OAR dose to the bladder came from a plan with another small target (HRCTV = 15.74 cm^3). This agrees with our expectation since the dose modulating capabilities of the DMBT tandem are the strongest for small targets within 2-3 cm from the tandem. The spatial dose distribution was also more conformal to the target as seen in Figures 31-35. In many cases the visual improvement in the 100% isodose line for the bladder and sigmoid was apparent. The new dose 100% isodose line retained a similar shape as the original while omitting areas of overlap with OAR. In addition, the original plan's pear-shape dose distribution which has been associated with positive clinical outcomes was retained while using all DMBT tandem models. Results representing the total dose (EQD2) reductions by all 9 DMBT tandem models are presented in Table 6. It is shown that significant reductions in total dose (EQD2) was achievable

for all OARs using any DMBT tandem model. As we expected the largest and smallest total dose (EQD2) reductions came from the thicker (models 8 & 9) and thinner (models 1 & 2) DMBT tandem models respectively. The DMBT tandem proved that it could successfully lower the total dose of previously failing OAR to below their total dose limits. Significant results such as those presented in Tables 7-8 suggest that the model of DMBT tandem isn't necessarily important when it comes to lowering the EQD2 as all model demonstrated similar results. Therefore, more care can be taken into selecting the correct sized tandem based on the patient's anatomy. However; the slight increase in modulation from a thicker DMBT tandem may be necessary when the predicted total dose (EQD2) borders its recommended limit. Significant reductions in the recto-vaginal and vaginal dose reference points were achieved by all models. The greatest improvements came from the thicker (models 8 & 9) DMBT tandem models while the smallest improvements came from the thinnest (model 1) DMBT tandem model. These significant reductions are likely to decrease the probability of developing vaginal morbidity for surviving cervical cancer patients. Lastly, comparisons of the total treatment times between the original and DMBT tandem plans were of concern. One limitation of DMBT tandem is the additional treatment time dedicated to transferring the source between each of the six channels. In addition, it was noted that as the DMBT tandem thickness increases so to did the total treatment time. This is to be expected as increases in thickness imply more attenuating material which minimizes transmission through the backside and periphery of the source channels. This requires longer dwell times to create a given dose distribution. The thinnest (model 1) DMBT tandem was able to produce comparable treatment times to the original plan while the maximum average increase came from the thickest (model 9) with an additional time of roughly a minute and a half. While

this increase in modulation comes with a price in regards to time, the average total treatment time with each DMBT tandem model were clinically permissible.

6. Future Recommendations and Limitations

While our study examined a large variety of target sizes for simple intracavitary cases, it does not include all brachytherapy treatment techniques. As discussed previously, the use of interstitial needles results in increased invasiveness and is not ideal as their placement can be difficult due to a lack of adequate physician training as well as flexing of the needles in the vaginal tissue. In addition, symptoms such as swelling are associated with the use of needles. For these reasons, we recommend that intracavitary-interstitial cases be examined using the DMBT tandem in order to identify the extent to which the modulating capabilities of the tandem can replace the need for some or all needles. In addition, the DMBT tandem prototype in this study was designed to be straight while the uterine canal is curving. This makes the placement of the current dMBT tandem design infeasible without potentially perforating uterine tissue . This design was likely adopted for simplicity but in order for it to be a clinically viable option, a curving DMBT tandem must be designed and constructed.

7. Conclusion

24 cervical cancer treatment plans previously treated by brachytherapy using conventional tandems and rings or ovoids were replanned using each of the 9 DMBT tandem models. All DMBT tandem models exhibited the ability to significantly lower OAR doses compared to

conventional tandem plans while maintaining equivalent target coverage. As we expected, the thicker DMBT tandem models performed better in this sense than the thinner models by virtue of its slightly thicker tungsten-alloy material. There were no significant differences in performance between all DMBT tandem models suggesting that the selection of a moderate thickness tandem may be recommended for clinical use due to its ease of placement and adequate dose modulating capabilities. In addition, OARs that previously exceeded their total (EQD2) dose limits when the conventional tandem was used were lowered significantly below their limits when any of the DMBT tandem models were used. Plans with both small and large targets benefited from the use of the DMBT tandem. This has sparked interest into the extent of the tandem's performance for very large targets as the DMBT tandem could potentially eliminate the need for interstitial needles in such cases.

8. References

1. Kemikler G. History of Brachytherapy. *Türk onkoloji dergisi*. 2019;34. doi:10.5505/tjo.2019.1

2. de la Garza-Salazar JG, Morales-Vásquez F, Meneses-Garcia A. *Cervical Cancer*. 1st ed. 2017. Springer International Publishing; 2017. doi:10.1007/978-3-319-45231-9

3. Safaeian M, Solomon D, Castle PE. Cervical Cancer Prevention—Cervical Screening: Science in Evolution. *Obstetrics and gynecology clinics of North America*. 2007;34(4):739-760. doi:10.1016/j.ogc.2007.09.004

4. BURD EM. Human Papillomavirus and Cervical Cancer. *Clinical Microbiology Reviews*. 2003;16(1):1-17. doi:10.1128/CMR.16.1.1-17.2003

5. Kim HS, Song YS. International Federation of Gynecology and Obstetrics (FIGO) staging system revised: what should be considered critically for gynecologic cancer? *Journal of gynecologic oncology*. 2009;20(3):135-136. doi:10.3802/jgo.2009.20.3.135

6. Sadozye AH, Reed N. A Review of Recent Developments in Image-Guided Radiation Therapy in Cervix Cancer. *Current oncology reports*. 2012;14(6):519-526. doi:10.1007/s11912-012-0275-3

7. Perez CA, Grigsby PW, Castro-Vita H, Lockett MA. Carcinoma of the uterine cervix. II. Lack of impact of prolongation of overall treatment time on morbidity of radiation therapy. *International journal of radiation oncology, biology, physics*. 1996;34(1):3-11. doi:10.1016/0360-3016(95)00169-7

8. Barnes EA, Thomas G, Ackerman I, et al. Prospective comparison of clinical and computed tomography assessment in detecting uterine perforation with intracavitary brachytherapy for carcinoma of the cervix. International journal of gynecological cancer. 2007;17(4):821-826. doi:10.1136/ijgc-00009577-200707000-00011

9. Wolman I. Berek and Novak's Gynecology 15th Edition: Lippincott Williams and Wilkins, 2012, 1560 pp, Hardcover, Rs. 2659 on www.flipkart.com, ISBN-139788184736106, ISBN-10818473610X. The Journal of Obstetrics and Gynecology of India. 2014;64(2):150-151. doi:10.1007/s13224-014-0538-z

10. Philippe Lambin AK. Tumour Size in Cancer of the Cervix. Acta oncologica. 1998;37(7-8):729-734. doi:10.1080/028418698430115

11. Stehman FB, Bundy BN, Disaia PJ, Keys HM, Larson JE, Fowler WC. Carcinoma of the cervix treated with radiation therapy I. A multi-variate analysis of prognostic variables in the gynecologic oncology group. *Cancer*. 1991;67(11):2776-2785. doi:10.1002/1097-0142(19910601)67:11<2776::AID-CNCR2820671111>3.0.CO;2-L

12. Chino J, Annunziata CM, Beriwal S, et al. The ASTRO clinical practice guidelines in cervical cancer: Optimizing radiation therapy for improved outcomes. *Gynecologic oncology*. 2020;159(3):607-610. doi:10.1016/j.ygyno.2020.09.015

13. Serban M, Kirisits C, Pötter R, et al. Isodose surface volumes in cervix cancer brachytherapy: Change of practice from standard brachytherapy. *Radiotherapy and oncology*. 2018;129(3):567-. doi:10.1016/j.radonc.2018.09.002

14. Dimopoulos JC., Petrow P, Tanderup K, et al. Recommendations from Gynaecological (GYN) GEC-ESTRO Working Group (IV): Basic principles and parameters for MR imaging within the frame of image based adaptive cervix cancer brachytherapy. *Radiotherapy and oncology*. 2012;103(1):113-122. doi:10.1016/j.radonc.2011.12.024

15. Viswanathan AN, Erickson B, Gaffney DK, et al. Comparison and Consensus Guidelines for Delineation of Clinical Target Volume for CT- and MR-Based Brachytherapy in

Locally Advanced Cervical Cancer. *International journal of radiation oncology, biology, physics*. 2014;90(2):320-328. doi:10.1016/j.ijrobp.2014.06.005

16. Kirisits C, Lang S, Dimopoulos J, Berger D, Georg D, Pötter R. The Vienna applicator for combined intracavitary and interstitial brachytherapy of cervical cancer: Design, application, treatment planning, and dosimetric results. *International journal of radiation oncology, biology, physics*. 2006;65(2):624-630. doi:10.1016/j.ijrobp.2006.01.036

17. Pötter R, Kirisits C, Fidarova EF, et al. Present status and future of high-precision image guided adaptive brachytherapy for cervix carcinoma. *Acta oncologica*. 2008;47(7):1325-1336. doi:10.1080/02841860802282794

18. Lindegaard JC, Tanderup K, Nielsen SK, Haack S, Gelineck J. MRI-Guided 3D Optimization Significantly Improves DVH Parameters of Pulsed-Dose-Rate Brachytherapy in Locally Advanced Cervical Cancer. *International journal of radiation oncology, biology, physics*. 2008;71(3):756-764. doi:10.1016/j.ijrobp.2007.10.032

19. De Brabandere M, Mousa AG, Nulens A, Swinnen A, Van Limbergen E. Potential of dose optimisation in MRI-based PDR brachytherapy of cervix carcinoma. *Radiotherapy and oncology*. 2007;88(2):217-226. doi:10.1016/j.radonc.2007.10.026

20. Han DY, Webster MJ, Scanderbeg DJ, et al. Direction-Modulated Brachytherapy for High-Dose-Rate Treatment of Cervical Cancer. I: Theoretical Design. International

journal of radiation oncology, biology, physics. 2014;89(3):666-673. doi:10.1016/j.ijrobp.2014.02.039

21. Soliman AS, Owrangi A, Ravi A, Song WY. Metal artefacts in MRI-guided brachytherapy of cervical cancer. Journal of contemporary brachytherapy. 2016;8(4):363-369. doi:10.5114/jcb.2016.61817

22. Safigholi H, Han DY, Mashouf S, et al. Direction modulated brachytherapy (DMBT) for treatment of cervical cancer: A planning study with 192Ir, 60Co, and 169Yb HDR sources. Medical physics (Lancaster). 2017;44(12):6538-6547. doi:10.1002/mp.12598

23. Bergmark K, Åvall-Lundqvist E, Dickman PW, Henningsohn L, Steineck G. Vaginal Changes and Sexuality in Women with a History of Cervical Cancer. *The New England journal of medicine*. 1999;340(18):1383-1389. doi:10.1056/NEJM199905063401802

24. JENSEN PT, GROENVOLD M, KLEE MC, THRANOV I, PETERSEN MA, MACHIN D. Early-stage cervical carcinoma, radical hysterectomy, and sexual function: A longitudinal study. *Cancer*. 2004;100(1):97-106. doi:10.1002/cncr.11877

25. Kirchheiner K, Nout RA, Tanderup K, et al. Manifestation Pattern of Early-Late Vaginal Morbidity After Definitive Radiation (Chemo)Therapy and Image-Guided Adaptive

Brachytherapy for Locally Advanced Cervical Cancer: An Analysis From the EMBRACE Study. *International journal of radiation oncology, biology, physics*. 2014;89(1):88-95. doi:10.1016/j.ijrobp.2014.01.032

26. Kirchheiner K, Smet S, Jürgenliemk-Schulz IM, et al. Impact of Vaginal Symptoms and Hormonal Replacement Therapy on Sexual Outcomes After Definitive Chemoradiotherapy in Patients With Locally Advanced Cervical Cancer: Results from the EMBRACE-I Study. *International journal of radiation oncology, biology, physics*. 2022;112(2):400-413. doi:10.1016/j.ijrobp.2021.08.036

27. LIND H, WALDENSTRÖM A-C, AVALL-LUNDQVIST E, et al. Late symptoms in long-term gynaecological cancer survivors after radiation therapy: a population-based cohort study. *British journal of cancer*. 2011;105(6):737-745. doi:10.1038/bjc.2011.315

28. Kirchheiner K, Nout RA, Lindegaard JC, Haie-Meder C, Mahantshetty U, Segedin B, et al. Dose- effect relationship and risk factors for vaginal stenosis after definitive radio(chemo)therapy with image-guided brachytherapy for locally advanced cervical cancer in the EMBRACE study. Radiother Oncol. 2016;118:160-6.

29. Westerveld H, Kirchheiner K, Nout RA, et al. Dose-effect relationship between vaginal dose points and vaginal stenosis in cervical cancer: An EMBRACE-I sub-study. *Radiotherapy and oncology*. 2022;168:8-15. doi:10.1016/j.radonc.2021.12.034

30. Viswanathan ANAN, Beriwal SS, De Los Santos JJ, et al. The American Brachytherapy Society Treatment Recommendations for Locally Advanced Carcinoma of the Cervix Part II: High Dose-Rate Brachytherapy. *Brachytherapy*. 2012;11(1):47-52. doi:10.1016/j.brachy.2011.07.002

31. Chino J, Annunziata CM, Beriwal S, et al. The ASTRO clinical practice guidelines in cervical cancer: Optimizing radiation therapy for improved outcomes. *Gynecologic oncology*. 2020;159(3):607-610. doi:10.1016/j.ygyno.2020.09.015

32. Albuquerque K, Hrycushko BA, Harkenrider MM, et al. Compendium of fractionation choices for gynecologic HDR brachytherapy—An American Brachytherapy Society Task Group Report. *Brachytherapy*. 2019;18(4):429-436. doi:10.1016/j.brachy.2019.02.008

33. Viswanthan AN, Thomadsen BAmerican Brachytherapy Society Cer- vical Cancer Recommendations Committee. American Brachyther- apy Society consensus guidelines for locally advanced carcinoma of the cervix. Part I: general principles. Brachytherapy 2012;11:33–46.

34. Viswanthan AN, Beriwal S, De Los, Santos JF, et al. Ameri- can Brachytherapy Society consensus guidelines for locally ad- vanced carcinoma of the cervix. Part II: high-dose-rate brachyther- apy. Brachytherapy 2012;11:47–52.

35. Lee LJ, Das IJ, Higgins SA, et al. American Brachytherapy So- ciety consensus guidelines for locally advanced carcinoma of the cervix. Part II: low-dose-rate and pulsed-dose-rate brachytherapy. Brachytherapy 2012;11:53–57.

36. Chino J, Annuziata CM, Beriwal S, *et al.* Radiation therapy for cervical cancer: executive summary of an ASTRO clinical practice guideline. *Pract Radiat Oncol* 2020;10:220–234.

37. Serban M, Kirisits C, Potter R, *et al.* Isodose surface volumes in cervix cancer brachytherapy: change of practice from standard (point A) to individualized image guided adaptive (EMBRACE I) brachytherapy. *Radiother Oncol* 2018;129:567–574.

38. Potter R, Tanderup K, Schmid MP, *et al.* MRI-guided adap- tive brachytherapy in locally advanced cervical cancer (EM- BRACE-I): a multicentre prospective cohort study. *Lancet Oncol* 2021;22:538–547.

39. Han DY, Webster MJ, Scanderbeg DJ, et al. Direction-Modulated Brachytherapy for High-Dose-Rate Treatment of Cervical Cancer. I: Theoretical Design. *International journal of radiation oncology, biology, physics*. 2014;89(3):666-673. doi:10.1016/j.ijrobp.2014.02.039

40. Perez-Calatayud J, Ballester F, Das RK, et al. Dose calculation for photon-emitting brachytherapy sources with average energy higher than 50 keV: Report of the AAPM and ESTRO. *Medical physics (Lancaster)*. 2012;39(5):2904-2929. doi:10.1118/1.3703892

41. Angelopoulos A, Baras P, Sakelliou L, Karaiskos P, Sandilos P. Monte Carlo dosimetry of a new 192Ir high dose rate brachytherapy source. *Medical physics (Lancaster)*. 2000;27(11):2521-2527. doi:10.1118/1.1315316

42. Ballester F, Puchades V, Lluch JL, et al. Technical note: Monte-Carlo dosimetry of the HDR 12i and Plus 192Ir sources. *Medical physics (Lancaster)*. 2001;28(12):2586-2591. doi:10.1118/1.1420398

43. FOWLER JF. 21 years of Biologically Effective Dose. *British journal of radiology*. 2010;83(991):554-568. doi:10.1259/bjr/31372149